UNIVERSIDADE DE LISBOA

FACULDADE DE CIÊNCIAS

DEPARTAMENTO DE BIOLOGIA VEGETAL

3D visualization of tissue specific vascular patterns for endothelial cell polarity analysis

Ana Alexandra Russo

Mestrado em Biologia Molecular e Genética

Dissertação Orientada por:
Cláudio Areias Franco, PhD
Maria Margarida Ramos, PhD

2016

Acknowledgments

Antes de mais, quero agradecer ao meu orientador de mestrado Cláudio Areia Franco por me dar a oportunidade de realizar o meu estágio de mestrado no laboratório de Morfogénese Vascular no Instituto de Medicina Molecular. O Cláudio permitiu-me ganhar experiência em várias áreas, através de todas a experiências realizadas ao longo do meu estágio. Através deste estágio aprendi a trabalhar com ratinhos e células. Realizei imensas genotipagens, aprendi a perfundir ratos e a extrair órgãos, a dissecar retinas, um órgão bastante utilizado neste laboratório para o estudo da vasculatura e aprendi a trabalhar em cultura celular na tentativa de acompanhar a vasculogénese e angiogénese *in vitro*. Apreciei bastante o trabalho que realizei neste laboratório e gostei bastante das experiências que realizei. Agradeço ao meu orientador por me ter permitido realizar estes diversos tipos de experiências.

Seguidamente agradeço ao Pedro Barbacena com quem partilhei a bancada e me guiou durante o ano, auxiliando as minhas experiências e meu ajudou na escrita de tese e em muitos outros trabalhos de apresentação em *lab meetings*. Foi o Pedro quem esteve a acompanhar-me mais de perto todo o progresso das minhas experiências e me ajudou a resolver alguns problemas que foram decorrendo. Ensinou-me a trabalhar com o software de processamento de imagem Fiji e esteve ao meu lado durante as minhas primeiras aquisições de imagem no Confocal. Ensinou-me a trabalhar com a bomba de perfusão para poder realizar as experiências de *microfluidics*. Foi o Pedro quem realizou as perfusões em todos os ratinhos que usei nestas experiências.

Agradeço à Anna Pezzarosa a quem pedi auxílio na resolução de problemas de processamentos de imagem e me fez a medição das dimensões dos núcleos das células endoteliais e fez análise de intensidades de fluorescência. Foi a Anna quem me fez a medição de índices de refração no Instituto Superior Técnico.

Agradeço especialmente ao técnico de *bioimaging* António Temudo pela formação que me deu no Confocal 880 e no Lightsheet, tendo ajudado a adquirir varias imagens de retinas. Agradeço por ter passado horas a ajudar-me a processar imagens adquiridas no lightsheet, a ensinar-me a trabalhar com os *softwares* de processamento e visualização de imagem Arivis 4D Vision® e Imaris®. Resolveu-me imensos problemas que surgiram devido ao peso dos ficheiros que impediam o processamento.

Agradeço à Aida por me ensinar a trabalhar em cultura celular, tendo sido extremamente rígida comigo, pois é muito fácil contaminar qualquer instrumento de uso comum podendo comprometer o trabalho dos outros. Acompanhou-me durante os ensaios de *coating* de células com fibrinogénio.

Foi a Aida quem me ensinou a trabalhar com as retinas e a colocá-las em lamelas para observação no microscópio.

Agradeço em seguida aos meus amigos de faculdade, alguns deles me seguiram para o mesmo mestrado, e amigos mais antigos com quem falo bastante ainda hoje e me acompanharam ao longo deste ano atarefado e aturaram as minhas mudanças de humor e cansaço de trabalho e mesmo assim arranjaram tempo para se encontrar comigo para discutir e desanuviar as frustrações de falta de resultados.

Agradeço muito aos meus colegas de música que me proporcionaram noites de ensaios e concertos que desnuviaram bastante, sempre cheias de palhaçada, risos e música da mais bela sem a qual eu não consigo passar.

Finalmente agradeço aos meus Pais, irmã e irmão e avós por estarem comigo e aturarem-me em todos os aspectos e por terem interesse no que faço, mesmo que não percebam nada do que estou a falar.

Muito obrigada

Ana Russo

Abstract

Tissues require specialised vascular beds to perform their functions. The main mechanisms driving organ-specific vascular remodelling are poorly understood. VEGF is the main regulator of sprouting angiogenesis, inducing the expansion of the primitive plexus into a highly branched network. Shear-stress, on the other hand, is the remodelling inducer, that is very important for patterning. VEGF-driven angiogenesis generates a highly branched network where some vessels are not well perfused. During the remodelling and maturation of the angiogenic network, vessel regression eliminates superfluous vessels. Thus, through vascular remodelling the network becomes hierarchically organized and functional. It is known that different tissues have different VEGF distribution patterns and different haemodynamic specificities. Given that both VEGF and shear stress are endothelial cell polarity inducers, we propose that these two factors compete for establishing the endothelial cell polarity axis and that this competition may influence organ-specific patterning. To be able to tackle this question, we decided to develop methods to visualize vascular patterns of whole-organs, stained not just for vessels, but for endothelial cell nucleus and Golgi apparatus as well, in order to assess the endothelial cell polarity and correlate it with VEGF levels in those tissues. In order to visualize deep into tissue we had to optically clear the different tissues (make them transparent). Most of the clearing protocols damage immunofluorescence stainings, so we focused on achieving a clearing protocol that would clear the tissue well while maintaining staining integrity, enabling us to make 3D image acquisition for polarity analysis. For large 3D imaging, the lightsheet microscope was used, for it is a system designed to allow imaging of whole cleared organs. Polarity analysis and correlation with flow and VEGF was not possible, since 3D networks were harder to analyse, but a successful clearing protocol for the specific polarity staining was achieved.

Keywords: Tissue clearing, Tissue patterning, Axial Polarity,

Resumo

A formação de uma rede vascular funcional e padronizada é crucial para o desenvolvimento e crescimento de todos os vertebrados. Qualquer disfunção na formação da rede vascular leva à patogénese de várias doenças como tumores, malformações arteriovenosas, aneurismas, entre outros.

Após a vasculogénese (formação de vasos a partir de precursores endoteliais), a angiogénese expande e remodela a vasculatura. Esta remodelação é um balanço entre *sprouting* e regressão de vasos que determina uma rede vascular hierárquica e funcional. Estudos recentes apontam para um

papel importante da motilidade e polaridade das células endoteliais no processo de morfogénese vascular. A polaridade celular consiste na distribuição assimétrica de proteínas e organelos dentro da célula, que permite definir estruturas e funções específicas em diferentes regiões da mesma célula. A distribuição assimétrica é estabelecida por complexos de proteínas que definem o eixo de polarização a jusante de factores extracelulares. As células podem estar polarizadas em vários eixos, como o eixo apico-basal ou anterior-posterior/axial. F*ranco et al.* definiram o posicionamento do Golgi em relação ao núcleo como eixo de polaridade axial nas células endoteliais.

O VEGF e o fluxo sanguíneo são dois reguladores importantes da polaridade axial das células endoteliais. O fluxo sanguíneo é importante para a padronização/remodelação da rede de vasculatura. Esta remodelação é o que leva à aquisição de padrões vasculares específicos em cada tecido. Este padrão/arquitetura de vasos é importante e bastante distinto entre órgãos, pois correlaciona-se com a função do tecido e a importância da circulação para essa função. As células endoteliais têm capacidade de sentir a fricção causada pelo fluxo sanguíneo, chamada de tensão de cisalhamento, traduzindo força em sinais bioquímicos mediante várias moléculas, incluindo PECAM1, VE-caderina, VEGFR2, PIEZO1 e cílios primários. O fluxo induz a polarização das células na direção contrária à do fluxo. Já o VEGF, um factor pró-angiogénico, induz também polarização das células endoteliais em direção a gradientes crescentes de VEGF. Notavelmente, durante o processo de angiogénese, a polarização induzida por estes dois factores é tendencialmente oposta. Com base nestas observações, formulámos a hipótese de que o VEGF e o fluxo sanguíneo estão em competição para estabelecer o eixo de polaridade das células endoteliais. Esta competição terá assim um impacto na orientação das células endoteliais, e consequentemente na morfogénese vascular e padronização. Esta questão tem ainda especial interesse pois sabe-se também que diferentes órgãos possuem níveis variados de VEGF, o que também é correlacionado com padrões vasculares próprios. Assim, o nível da competição entre o VEGF e o fluxo sanguíneo poderá ter um papel importante na definição dos padrões vasculares específicos a cada órgão.

Sabe-se que o complexo PAR (PAR-6/PAR-3/aPKC) define o eixo de polaridade de vários tipos celulares. Resultados preliminares mostram que este complexo regula a capacidade das células polarizarem em reação ao VEGF e ao fluxo sanguíneo. Desconhece-se, no entanto, as vias de sinalização que estabelecem a competição entre estes dois factores de polarização.

No estudo realizado pretendemos responder a duas questões: como decorre a remodelação de vasos em cada órgão que leva a uma arquitetura vascular específica? Terá o VEGF influência na polarização das células endoteliais contra o fluxo e essa influência alterna o padrão da vasculatura?

Para tentar responder a estas questões, técnicas de imagiologia foram usadas para determinar a polaridade das células endoteliais e morfologia da vasculatura em cada órgão, usando

técnicas de visualização 3D e métodos que permitem aumentar a transparência dos tecidos. A transparentização consiste em diminuir a dispersão de luz que ocorre nos tecidos, o que os torna opacos, de modo a igualar os índices de refração do meio com o índice de refração médio do tecido. As técnicas dividem-se em dois grandes grupos: técnicas que utilizam solventes orgânicos e técnicas aquosas. Dentro destes grupos, os métodos para obter tecidos transparentes consistem em imersão simples dos tecidos para igualar os índices de refração ou remoção de lípidos. Neste âmbito várias técnicas de transparentização foram testadas e otimizadas na tentativa de compatibilizar a marcação com fluorescência das estruturas com a técnica aplicada.

Os primeiros testes revelaram sensibilidade da marcação dos vasos com anticorpos que marcavam receptores de membrana. Estas técnicas removiam lípidos pelo que se justificava a ausência de marcação, sendo que algumas destas foram excluídas. A técnica que melhor conciliou a capacidade de transparentização e com a compatibilidade com a marcação com anticorpos (isto após algumas modificações ao protocolo original) foi a técnica designada Protocolo 2 que foi uma adaptação do protocolo CUBIC. Após a otimização das técnicas e da marcação com anticorpos específicos que se estavam a utilizar, procedeu-se à adição do anticorpo para marcar o complexo de Golgi ao cocktail de anticorpos. A dificuldade na marcação do complexo de Golgi e do núcleo residiu na reação cruzada que havia nos anticorpos secundários, uma vez que os primários foram criados na mesma espécie. A visualização das três entidades era compatível com o protocolo de transparentização que se estava a utilizar, mas as imagens obtidas podem ser muito confusas devido à presença de sinal de golgi em dois canais. No entanto o tamanho dos dois organelos é distinto, permitindo a diferenciação entre os dois.

Durante a otimização do protocolo, foram feitos testes ao sistema de microscópio de *lightsheet* que seria o microscópio especializado para obter grandes imagens tridimensionais sem ter de haver seccionamento físico das amostras. Este microscópio contém uma câmara onde fica suspensa a amostra mergulhada num líquido de índice de refração compatível com o índice médio da amostra após ser transparentizada. Testes iniciais usando retinas de ratinho revelaram a dificuldade em trabalhar com ficheiros obtidos neste sistema, uma vez que uma aquisição de uma retina inteira daria origem a um ficheiro de 1Tb, praticamente impossível de processar nas estações de trabalho presentes no instituto. Após alguns testes, passou-se para aquisição de órgãos. Notoriamente a aquisição da vasculatura do cérebro teve sucesso. O cérebro é facilmente transparentizado e a vasculatura é bastante fácil de adquirir em *lightsheet*. Para fazer reconstrução 3D da vasculatura usando *lightsheet*, o cérebro é um bom candidato. Já o rim, não transparentiza tão facilmente como o cérebro e a vasculatura é altamente densa, sendo que o *lightsheet* não é capaz de resolver a estrutura típica do rim que é o glomérulo. Possivelmente o rim terá de ser

adquirido em confocal, mas este microscópio tem uma distância de trabalho limitada não permitindo adquirir grandes estruturas em 3D. O intestino tem a estrutura especializada da vilosidade que é facilmente adquirida em confocal.

Com a imunofluorescência do complexo de Golgi e do núcleo obtida, traçam-se os vetores de polaridade das células utilizando um script do MatLab escrito especificamente para desenhar vetores de polaridade. Porém o script funciona bem assumindo que a rede vascular é bidimensional, como nas retinas, o que não acontece em órgãos uma vez estes apresentam uma rede vascular tridimensional complexa. Do mesmo modo, simular o fluxo também se torna complicado para estas estruturas. Como tal não se pôde correlacionar a polaridade com o fluxo sanguíneo, nem correlacionar com VEGF.

A adaptação de um protocolo de transparentização compatível com as marcações para os vasos, núcleos e complexo de Golgi foi um passo essencial para se poder visualizar órgãos e traçar vetores de polaridade, para futuramente se poder tirar resultados mais conclusivos em relação à orientação das células em relação ao fluxo e a influência do VEGF para a mesma polarização e potencialmente para a padronização dos vasos específica de cada órgão.

Palavras-chave: Transparentização, Padronização em tecidos, Polaridade Axial

Abbreviations

A4P0 - Acrylamide 4%, PFA 0%

ADPKD - Autossomic Dominant Polycistic kidney disease

AKT – or PKB is Protein Kinase B

ANG - Angiopoetin

aPKC - atypical Protein Kinase C

ARP2/3 – actin-related proteins 2 and 3

CBB – Cláudio's Blocking Buffer

Cdc42 – Cell Division Cycle 42

CUBIC – Clear, Unobstructed Brain Imaging Cocktails and Computational analysis

DBE - Dibenzyl Ether

DCM - Dichloromethane

DLG - Discs large

DLL4 - delta-like 4

DMSO - Dimethyl sulfoxide

Dvl - Dishevelled

EC – Endothelial Cell

ECM - Extracellular Matrix

ERG – (erythroblast transformation-specific*)-related gene*

ERK5 - Extracellular-signal-Regulated Kinase 5

FRUIT - Fructose and urea induced transparency

GEF - Guanine Exchange Factors

GTPase – Guanosine TriPhosphate hydrolase

GOLPH4 – Golgi Phosphoprotein 4

iDISCO - immunolabeling-enabled three-Dimensional Imaging of Solvent-Cleared Organs

Hh - Hedgehog

ICAM - Intercellular Adhesion Molecule

KLF2 – Krüppel-LikeFactor 2

LGL - Lethal giant larvae

MAPK – Mitogen-Activated Protein Kinase

MIP – Maximum Intensity Projection

MTOC - Microtubule-Organizing Center

Ncx1 - sodium/calcium exchangers

NF-kB - Nuclear Factor kappa-light-chain-enhancer of activated B cells

NICD - Notch intracellular domain

NO – Nitric Oxide

NP40 - Nonyl Phenoxypolyethoxylethanol

NRP1 - Neuropilin 1

PACT - Passive clarity technique

PALS1- (protein associated with LIN-7)-1

PAR - Partitioning-Defective

PATJ - PALS1- associated tight-junction protein

PC - Polycystin

PCP – Planar Cell Polarity

PDGF – Platelet-Derived Growth Factor

PDMS - Poly(Dimethylsiloxane)

PECAM1- Platelet endothelial cell adhesion molecule 1

PEG - Polyethilene Glycol

PI3K - Phospho-inositide 3-Kinase

PIGF – Placental Growth Factor

Rac1 – Ras-related C3 botulinum toxin substrate 1

RBP-Jκ - recombination signal-binding protein 1 for Jκ

RhoA - Ras homolog gene family, member A

RIMS – Refractive Index Matching Solution

ROBO - Roundabout gene family

SC - Stalk Cell

SRF – Serum Response Factor

Src - Proto-oncogene tyrosine-protein kinase

TC - Tip cell

TDE - 2,2'-thiodiethanol

THF – Tetrahydrofuran

TIE - Tyrosine kinase with immunoglobulin-like and EGF-like domains

WASP - Wiskott–Aldrich syndrome protein

WAVE - WASP family verprolin-homologous protein

Wnt - Wingless

VCAM - Vascular Cell adhesion Molecule

VE-cadherin - Vascular Endothelial cadherin

VEGF-A - Vascular Endothelial Growth Factor A

vSMCs - Vascular Smooth-Muscle Cells

VMC – Vascular Mural Cells

Index

Index of Figures

Index of Tables

Chapter I - Introduction

The vertebrate vasculature forms an extensive branched network of blood vessels that supplies tissues and organs with nutrients and oxygen. This network, also known as vascular plexus, needs to be functional and patterned for correct embryonic development, tissue growth and organ physiology. Any dysfunction or mis-patterning of this network triggers angiogenic pathologies such as tumors, malformations and aneurisms. [1–3]

I.1. Blood vessel formation

During embryonic development, endothelial cell (EC) precursors, called angioblasts, migrate and assemble into a primitive vascular network through a process known as vasculogenesis or *de novo* vessel formation. These precursors undergo cell differentiation and specification into a venous or arterial fate in a genetically programmed and haemodynamic dependent way. Following vasculogenesis, the primitive vascular network is expanded through sprouting angiogenesis, creating a highly branched network. This network is then remodeled, a process driven by blood flow, and that gives rise to a more functional and hierarchically organized vascular system. Recruitment of mural cells (VMC) and vascular smooth-muscle cells (vSMCs) stabilizes the vessels and promotes their maturation[1,2]. In adulthood, ECs remain in a quiescent state and normally angiogenesis does not occur except in few situations such as wounding, organ regeneration, menstrual cycle, or in some pathological events[4]. This is tightly controlled by a proangiogenic/antiangiogenic balance. Thus, angiogenesis is a dynamic remodelling process of expansion and regression, until the final patterned network is achieved.

I.1.1. Sprouting Angiogenesis

Sprouting angiogenesis can be described as a collective cell migration event. In this type of migration, cells are structurally and functionally connected (through cell junctions) and the migrating cohort remains attached to the parent vessel. Additionally, polarity and 'supracellular' organization are both necessary to achieve coordinated and directed movement[5].

Sprouting angiogenesis is mainly triggered by **V**ascular **E**ndothelial **G**rowth **F**actor VEGF. Among the types of VEGF (from A to E and PIGF)[4], the most important for vascular development is VEGFA. Knocking out just one copy of this factor is lethal for the embryo[6,7]. VEGFA gives rise to several isoforms via alternative splicing. The differential distribution of VEGFA isoforms, in particular the heparin-binding isoforms 164 and 188, generate a gradient that triggers directional vessel growth[8]. During the migratory process, and when higher levels of exogenous VEGFA are detected, a particular type of EC is specified to lead the new sprout. These are called endothelial tip cells (TC) and they have a unique morphology and genetic signature, expressing high levels of PDGF-B, VEGFR2 and VEGFR3, NRP1, DLL4, amongst other genes[9] (Figure 1). The delta-like (DLL)4–Notch

signaling laterally inhibits TC fate in adjacent ECs. TCs have an invasive behavior that is promoted by the loosening of adherent junctions such as VE-cadherin (**V**ascular **E**ndothelial cadherin), by metalloproteinase-mediated degradation of extracellular matrix (ECM) and through cytoplasmatic protrusions, called filopodia and lamellipodia, which are responsible to sense both attracting and repulsive signals and to guide the TC. VEGF triggers this behavior through activation of the transmembranar receptor kinase VEGFR2, which activates several pathways such as MAPKs, phosphoinositide 3-kinases (PI3Ks), SRF (serum response factor), AKT and GTPases. Collectively, VEGFR2 signalling contribute to EC proliferation, filopodial extension and chemotaxis.

The TCs are followed by endothelial stalk cells (SC), which maintain the connection to the parent vessel and establish vessel lumen[1,10] (Figure1). The tip and stalk phenotypes are not definitive, ECs can switch between these states, so that the fittest cell initiates the sprouting[11]. The phenotype selection is mainly triggered by the DLL4-Notch lateral inhibition (as mentioned earlier). Notch and VEGF are opposing signals, the first is an inhibitor of sprouting, whereas the second induces sprouting. VEGF induces TC state but also acts as an upstream regulator of DLL4 expression (a Notch ligand), so cells that have higher VEGF signalling have decreased Notch signalling, but activates Notch in neighbouring cells. The Notch signalling in turn negatively regulates VEGFR in juxtaposed EC, leading to a decrease in the sensitivity of EC to VEGF, thereby inhibiting TC phenotype in cells adjacent to TCs[1]. When Dll4-Notch receptor interacts with its ligand on the adjacent cells (Notch1) there is a conformational change that leads to cleavage of the Notch

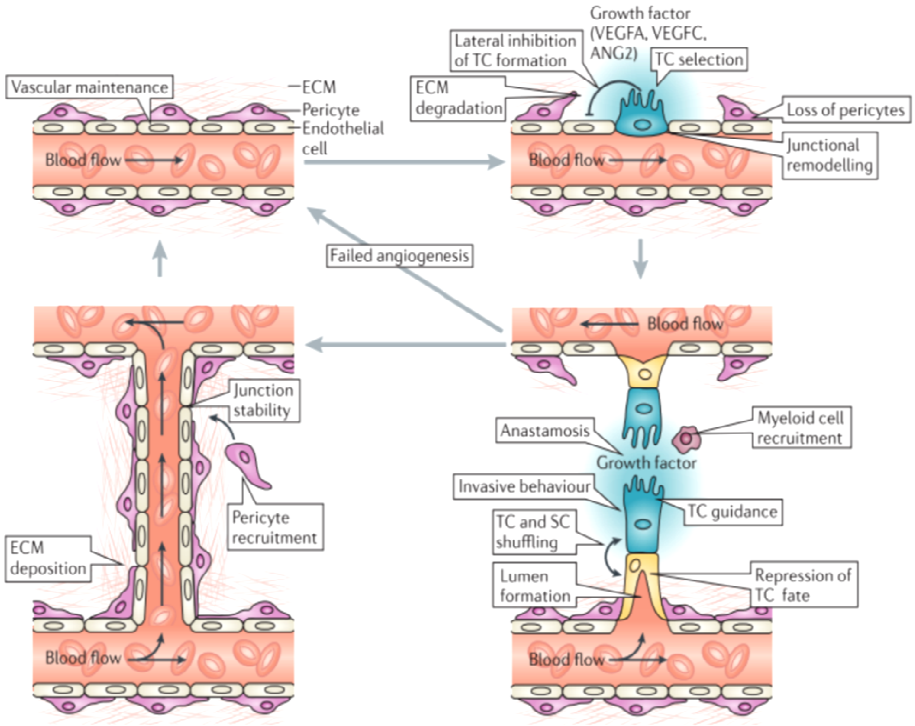

Figure 1 - Schematic representation of sprouting angiogenesis. From a quiescent state, cells sense pro-angiogenic factors, such as VEGF-A, VEGF-C and Angiopoetin-2, which induces sprouting. EC compete for TC (tip cell) fate and once the TC is selected it will begin to lead the sprout. VEGF-A takes the role of guiding the TC filopodia extensions. The SC (stalk cell) will follow the TC and maintain the connection to the parent vessel. Once the TC encounters another TC from another sprout they will merge in a process called anastomosis. The stalk cells are responsible for lumen formation. The fusion of the two sprouts gives rise to one continuous and unobstructed vessel[1].

intracellular domain (NICD). NICD translocates to the nucleus associating to RBP-Jκ (recombination signal-binding protein 1 for Jκ), thereby activating the transcription. Notch downregulates VEGFR2 and VEGFR3, but positively regulates VEGFR1 (Flt1). The soluble form of this receptor (sFlt1) serves as a decoy receptor that binds to VEGFA, clearing the free ligand from the environment and preventing it from binding to VEGFR2, therefore functioning as a negative regulator[12,13]. The communication between the two major pathways in sprouting angiogenesis, Notch and VEGF, is important for vascular patterns.

After the selection process, the sprout is guided by a VEGF gradient. When two vascular branches meet, they merge through anastomosis and during this process the TC lose their motility, form EC-EC junctions and are incorporated in the newly branched vessel, generating a continuous unobstructed lumen[1].

I.1.1.1. VEGF induced Polarization

VEGFA binding to VEGFR2 triggers the TC phenotype but also promotes cytoskeleton rearrangements, in order to establish front-to-rear polarization, and by extending the filopodia and lamellipodia. Cdc42 activation via VEGFR2 drives filopodia formation and regulates polarization, while Rac1, also activated by VEGFR2, controls lamellipodia. The front-to-rear polarization is essential for the tip cell to guide the emerging sprout. VEGF binding to its receptors in combination with Slit2/ROBO1 signalling regulates EC polarization, through the adapter protein NCK. Absence of ROBO1 impairs cell polarity, as measured by the random positioning of the Golgi, and abolish cdc42 response to VEGFA and Slit2, because ROBOs are essential for VEGF-mediated Rac1 activation[14].

I.1.2. Vascular Remodelling

Angiogenesis is not just sprouting. The tissue specific vascular formation undergoes two phases: first the formation of the primary capillary plexus through extensive branching, the second, vascular growth and remodelling (Figure 2A). Remodelling is an important event in vascular network formation. Remodelling takes place when vessels start being perfused with blood, and this perfusion will induce activation of signalling pathways, modifying gene expression in EC, such as Ncx1, N-cadherin and myosin light chain 2a[15]. Three cellular processes are important for remodelling: cell proliferation, cell migration and ECM production/degradation[15]. During this event, changes in lumen diameter and vessel wall thickness will suit local tissue needs[16], as well as regression of less perfused vessels, as a response to reduced blood flow. Also artery-vein specialization takes place and this specialization contributes for vessel diameter increase and flow normalization[17]. Another event that is considered remodelling is microcirculation rarefaction (loss of capillary area) that occurs in hypertension. This might be responsible for an avascular zone in the peri-arterial space. This lack of

capillarity increases with the vessel caliber. This is more frequent in arteries than in veins, possibly indicating sufficient oxygenation in the peri-arterial zone.

The heterogeneity of EC gene expression profile and signalling permits different responses to the environment, allowing the construction of different vascular beds that are specific for each tissue, depending on their function and the importance of the blood flow for their performance. It is known that the VEGF expression is triggered by hypoxia, but different tissues respond differently to hypoxia. The response during hypoxia, later determines the level of oxygenation of the specific tissue after angiogenesis, since VEGF not only is important for sprout guidance, but for establishment of fenestrations in quiescent state[18]. Therefore, the levels of VEGF are different in each organ, for instance in liver, in normoxic conditions, VEGF is equally distributed and this constitutive expression is responsible for high permeability of EC. Kidney seems to have higher VEGF expression in the glomeruli, and low level in periglomeruli cells. In brain, however, there seems to be low levels of VEGF, and this is consistent with the brain endothelium forming the blood brain barrier (BBB). Exchanges in this case happen not through fenestrations, but through specialized transporters in the EC membrane. This restricted patterned of VEGF distribution somehow, influences patterning in tissue-specific vascular beds[18].

Intussusception is a less understood remodeling process that can lead to microvascular growth, arborization and branching remodeling. Intussusceptive microvascular growth is a faster alternative to sprouting in which, instead of degradation of the basement membrane, migration and

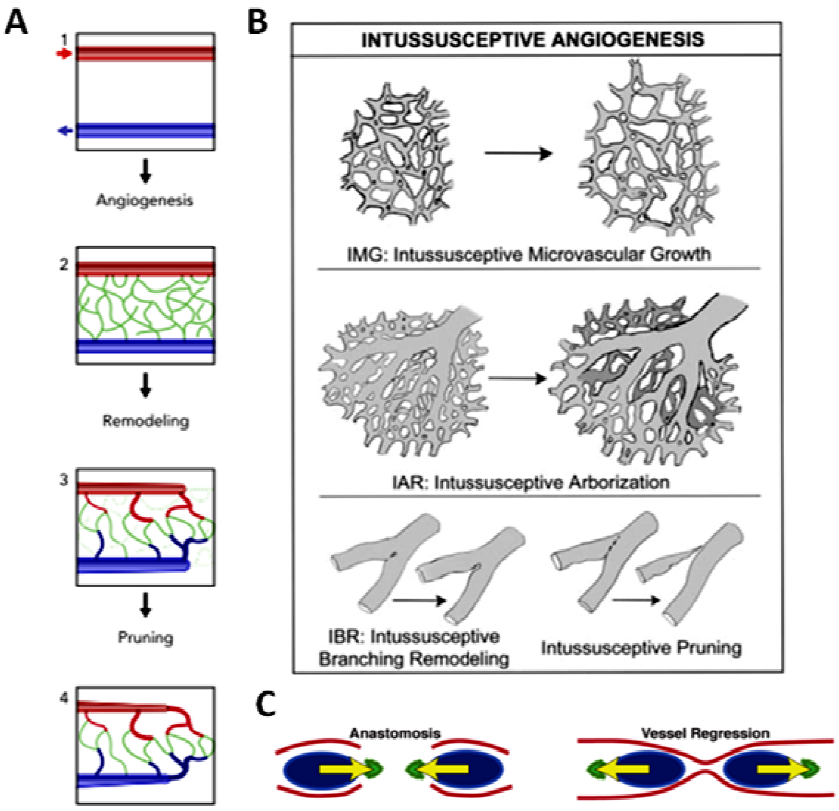

Figure 2 - Vascular Remodelling Events. A) Development of vascular network. After vasculogenesis, sprouting angiogenesis expands the network. Remodelling and pruning will drive the formation of an organized and hierarchical network[66]. B) The three intussusceptive processes of microvascular growth, arborization and branching and remodelling. These vessels will regressl[19]. C) Vessel regression through reversed anastomosis. Shear stress induces polarization of EC leading to a migration event of EC towards higher shear stress. In green is the Golgi apparatus and in blue the nucleus. The arrow represents the axial polarity measured by the positioning of the Golgi apparatus to the nucleus[21].

proliferation, the vessels simply split through the formation of “vertical pillars” inside the vessels that dilate and eventually lead to the splitting (Figure 2B)[19]. The regulatory mechanisms underlying the formation of these pillars remain unknown. Branching remodelling essentially works in order to achieve the ideal of the Murray law, which states that the cost of transporting blood can be minimized by enlarging the vessel’s diameter[20], by optimizing the blood flow distribution. Branching remodelling geometrically rearranges the network using the formation of “pillars” in the proximity of branching points.

In an extensive vessel network, blood fluid will not reach all vessels equally; therefore, some vessels will be less perfused. The highly sprouted network is formed because EC use anaerobic metabolism rather than the oxidative one and when glucose levels do not meet the cell requirements, due to the low energetic income from glycolysis, they switch to oxidative metabolism. For the glycolytic pathway to pair up with oxidative metabolism, ECs go from quiescent to proliferating and migrating state[11]. Regression (or vessel pruning) is a process that modifies the vascular network by removing less perfused blood vessels. Initially, it was proposed that the main driver for this regression event was EC apoptosis, however recent studies reveal that instead of undergoing apoptosis, ECs migrate and incorporate into more active vessels, enlarging them[21,22] (Figure 2A and 2C). Apoptosis drives vessel regression in pupillary membrane, however it is not the main driver of regression. This recent hypothesis states that the regressing vessel goes through a, somehow similar to, reversed anastomosis process. The described process for regression follows four steps: selection, lumen stenosis, EC retraction and resolution of the regressing vessel[21]. Apoptosis can be observed if the migratory EC fail to integrate the active vessel.

I.1.2.1. Shear-stress induced polarization

The key regulator of the remodelling event is blood flow[23], and ECs have the capacity to sense variations in this flow by sensing variations in shear stress, using surface proteins[24]. Shear stress is the frictional force per unit area and it is parallel to blood flow, proportional to the viscosity and blood velocity and it is the main driver of embryonic morphogenesis of heart and blood vessels[24]. When shear stress is strong enough it will induce polarization of EC against blood flow. The EC of low perfused vessels will be able to sense this higher blood flow through the neighbouring cells, resulting in polarization towards the same way, towards higher shear stress. In zebrafish, the axial polarity (measured through the positioning of the Golgi apparatus) correlates with directional cell migration (Figure 2C). The EC polarization results in a net movement of cells from a low-flow branch (which regresses) to high-flow branch (which enlarges)[21].

The development of the aortic arch vessels occurs due to the action of blood flow that influences VEGF signalling, by inducing the expression of Krüppel-like factor 2 (KLF-2) and promotes

expression of microRNA 126 which increases VEGF signaling[1]. KLF-2 drives formation of stress fibers that align the cells in direction or the blood flow[25]. Blood flow is known to activate several pathways like phospho-inositide 3-kinase (PI3K), extracellular signal-regulated kinase 5 (ERK5/MAPK7) and NO pathways that promote EC survival. PECAM-1, VE-cadherin and VEGFR2, together comprise a mechanosensory complex[23,24]. PECAM-1 directly senses shear stress and activates Src, VE-cadherin functions as an adaptor that brings VEGFR2 closer to PECAM-1 in order to be transactivated by Src. Activated VEGFR2 recruits PI3K that will activate several downstream signalling pathways, specifically the conformational activation of integrins pathway that leads to binding of ECs to the extracellular matrix (ECM). This binding will align the cells in the fluid direction via Rac, Rho and Cdc42. Rac1 activation also stimulates NF-kB activity that will trigger the expression of adhesion molecules like intercellular adhesion molecule (ICAM)-1, vascular cell adhesion molecule (V CAM)-1, endothelial (E)-selectin and platelet-derived growth factor (PDGF). Both NF-kB activation and ICAM1 expression are dependent on the integrin activation pathway[23,24]. Other known mechanosensors are the calcium channel called Piezo1[26] and the primary cilia which are specialized structures in the surface of the cell that can bend, upon flow, and trigger Ca^{2+} influx, through polycystins 1 and 2 at the membrane of the cilia[27].

I.2. Cell Polarity

Polarity is defined as an asymmetric distribution of surface proteins, channels, receptors, lipids and various cell contents. The asymmetry leads to a differential structure and function, allowing cellular processes to be regulated differentially across the cell. This inequality is achieved through, the so called polarity proteins, which define various types of cellular axis like apical-basal or anterior-posterior/axial[28,29,30] (Figure 3A). These domains are important to provide barriers between compartments, to maintain ion homeostasis, regulate cell migration and allow dispersion of cell content to daughter cells upon division[31]. The polarity proteins can translate signals, from internal or external sources, that result in cytoskeleton and vesicle transport changes.

The polarity existence is imperative for tissue morphogenesis and elongation[32]. Among the variety of polarity proteins, a well known family of proteins known as PAR (partitioning-defective), has important roles for the establishment of cell polarity, since it can regulate the actin and microtubule cytosqueleton[33]**.** Par proteins can associate and form complexes. The Par/aPKC complex is a conserved complex[28] that consists in an association between Par-3, Par-6 and aPKC protein (atypical protein kinase C). This complex on the other hand can interact with Par-1/Par-2 complex and amplify small initial polarity cues. The polarity establishment is achieved through distribution of Par-1/Par-2 complex to the basal domain and Par/aPKC complex to the apical domain and this asymmetric distribution occurs due to a cytoplasmatic flow generated from an asymmetric

actomyosin contraction[28] (Figure 3B). In mammalian cells, aPKC/Par6 plays a role in rearranging the microtubules, reorienting the microtubule-organizing center (MTOC)[28,34] which allows orientation of symmetric and asymmetric cell division, and is very important for tissue architecture and morphogenesis[32].

This complex contributes for the formation of intercellular junction, driving epithelial polarization. These localized complexes recruit proteins of the Rho family that are GTPases, such as RhoA, Cdc42 and Rac1 that are at the center of the mechanism - inducing polarization. When establishing cell polarity, cytoskeleton rearrangements are determined by local assembly of signaling complexes of Rho-GTPases family (Cdc42, Rho and Rac). Cdc42 and Rac1 are responsible for establishing front-to-rear and apico-basal polarity. Defects in these polarities will lead to defective anastomosis and remodeling. Cdc42 activates WASP (Wiskott–Aldrich syndrome protein) and Scar/WAVE complex that induces local assembly of actin filaments, via Arp2/3.

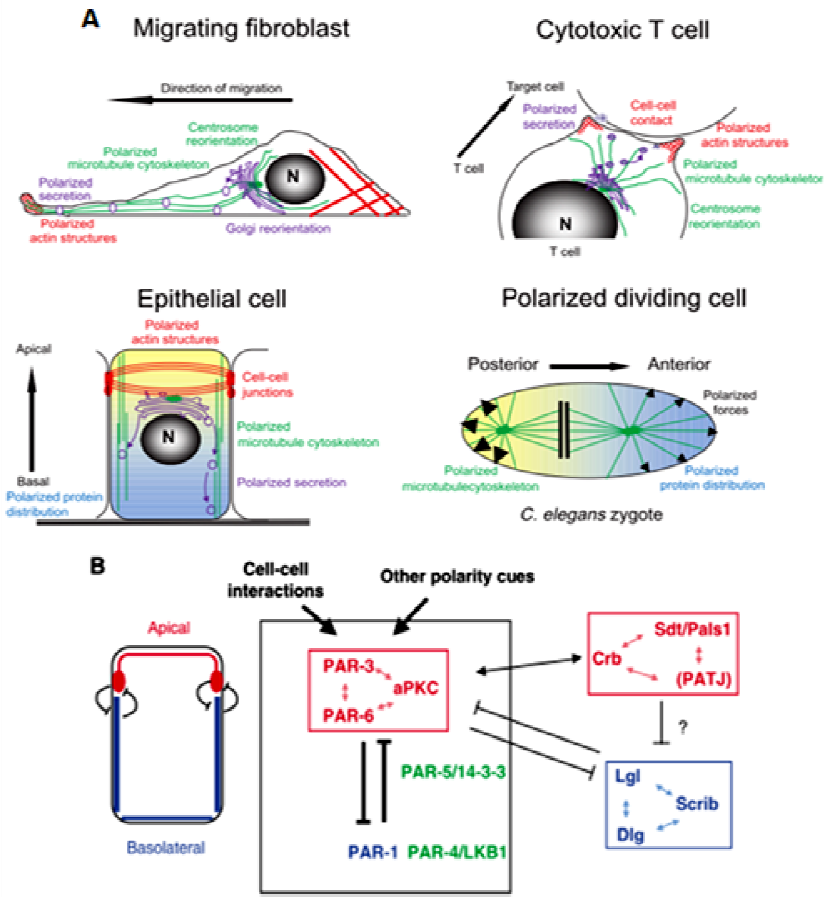

Figure 3 - Cell Polarity. A) Many types of cell polarity such as: front-to-rear (for migration), apico-basal, anterior-posterior polarities[34]. B) The establishment of apico-basal polarity that occurs through negative feedback loops between Par/aPKC complex, the remaining Par complexes and the Scribble and Crumb (Crb) complexes[28].

The Par complexes interact with other polarity proteins. Crumb complex comprises transmembrane protein Crumbs and scaffold protein PALS1 ((protein associated with LIN-7)-1) and PATJ (PALS1- associated tight-junction protein) and regulate epithelial polarity. Particularly Crumb3 determines the apical membrane and induces the formation of tight junctions. Scribble complex proteins comprise Scribble, Discs large (DLG) and Lethal giant larvae (LGL) proteins and determines the basolateral membrane and also align the mitotic spindle along the apico-basal axis. Scribble, Crumb and Par complexes interact by mutual exclusion to establish polarity[35](Figure 3B).

Another type of polarity proteins essential for tissue morphogenesis belongs to the planar cell polarity (PCP) pathway. PCP is important in multicellular tissues coordinating cell behavior across

the tissue, orthogonally to the apico-basal polarity, orienting them with the body axes. Clear examples of this polarity are the orientation of the hairy cells in the inner ear to the plane of the epithelium[36] and the orientation of the hairs on the mouse paw to the body axis[30]. A polarity cue is transmitted locally from one cell to another allowing all cells to respond as a unit. The main PCP signaling pathway is the non-canonical wnt (wingless) signaling in which a surface receptor frizzled, upon binding to Wnt5a or Wnt11 ligands, recruits the adaptor protein Dishevelled (Dvl) that activates Jun kinase-Rac-Rho pathway for cytoskeleton rearrangements[36]. Wnt5a, for instances, was found to be important for centrosome/Golgi reorientation. There are evidences of a link between Cdc42/Par6/aPKC and Wnt pathway for establishing microtubule polarity, particularly it was found that Dvl2 interacts with aPKC, but this interaction remains unclear[37].

I.3. Aims

ECs can sense the shear stress induced by blood flow and translate it to cellular signals. Blood flow is known to be the prompter of vessel pruning which is the major remodelling event in vascular morphogenesis. Blood flow induces polarization of ECs against the flow. Also, VEGF promotes angiogenic sprouting and it is known to induce EC polarization[9] (Figure 4). Thus, in a growing vascular network, such as the mouse retina model, there are two opposite drivers of EC polarization: in the sprouting front of the plexus, VEGF is the main driver of polarization, whereas, at the centre of the plexus, it is the blood flow that drives polarization. So what happens when these two factors are at balance? We hypothesize that VEGF and blood flow compete molecularly to control the cell polarity axis (Figure 4B). Because different tissues have specific vascular patterns and because it is known that they are presented with different levels of VEGF, not to mention that VEGFR2 plays

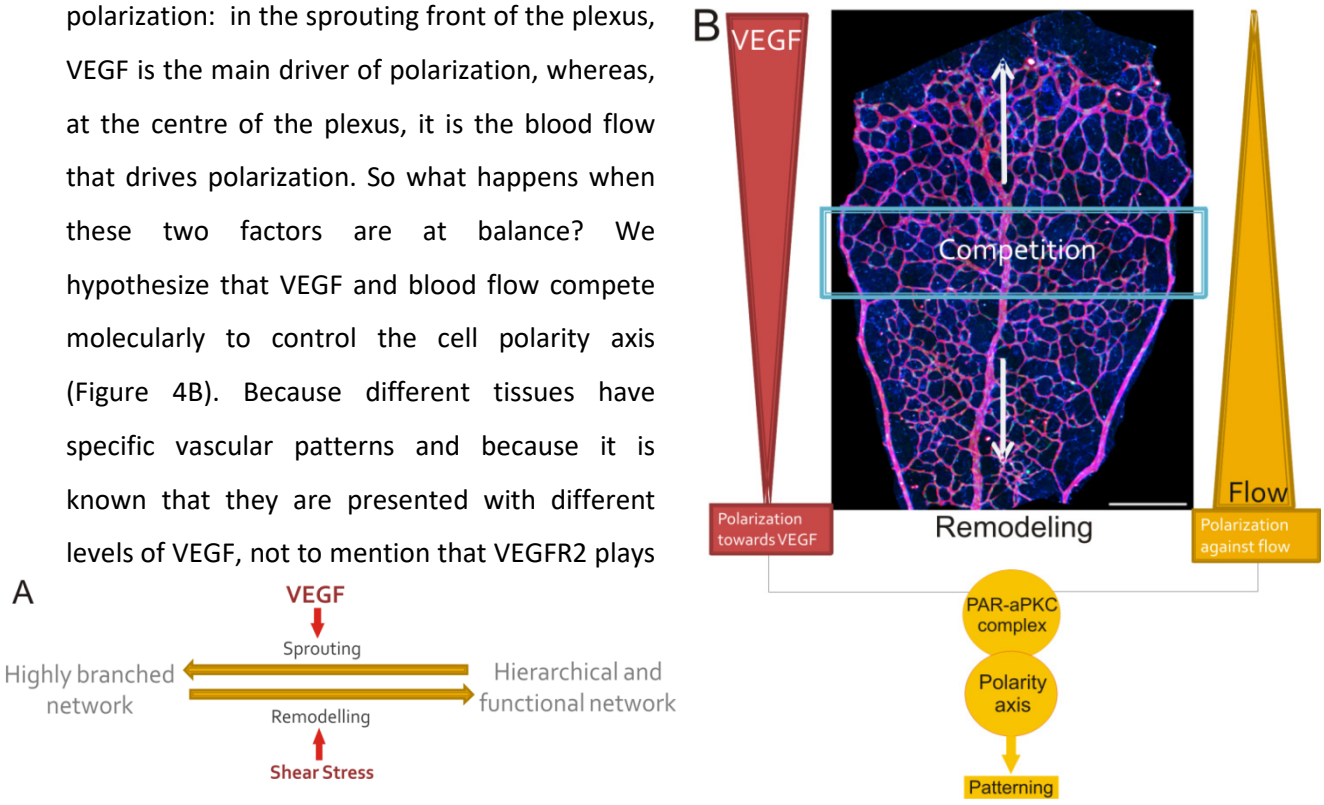

Figure 4 - Schematic representation of vascular network development. A) Angiogenesis as a sprouting and remodeling event controlled by VEGF and shear stress respectively. B) Cell polarity competition by VEGF and blood flow in retina plexus. At the sprouting front of the plexus VEGF is the dominant factor that induces polarization of endothelial cells towards it. At the center of the plexus, blood flow is the key factor regulating polarization against it. In the middle, both factors are at balance and so the hypothesis is that there may be a competition for establishing the polarity axis, possibly at Par/aPKC complex level. This competition may influence blood vessel morphology and vascular pattern.

a role not just in sprouting, but in shear stress sensing, it is also proposed that this competition may determine vessel patterning, which is important for tissue-specific functions. Several questions remain open in the field: What is the balance between VEGF and the flow signalling and when does one signal overcomes the other defining the polarity axis? Does VEGF influence polarization against the flow in an organ specific way and thereby influence vessel morphology? To be able to address these important questions we need to develop novel methods enabling 3D imaging in order to visualize vasculature in organs with single cell resolution for specific assessment of EC polarity patterns in whole organs. Thus, my master thesis work aims at adapting tissue clearing techniques to be able to use our own developed protocol to investigate EC polarity in 3D plexuses. Then, we aim at generating 3D maps of vascular networks of different organs and correlate blood flow, VEGF levels and endothelial cell polarity patterns to organ-specific vascular morphometric parameters.

I.3.1. Tissue Clearing

To get a 3D image of the vasculature, confocal microscopy and Lightsheet microscopy are used combined with techniques of tissue clearing. With the advent of optical sectioning microscopes, that allows imaging in depth, problems still arise from looking at thick tissue. The major problem is the translucence of biological tissues that lowers resolution and prevents deeper imaging[38]. This intrinsic appearance is due to multiple light scattering which consists in interference of absorbed and emitted light from neighbouring atoms. Organic materials tend to have this property due to their thickness and molecular heterogeneity, being the major source of scattering the membrane lipids. To overcome this problem, optical clearing methods were created in order to smooth the density of the scattering materials (by matching the refractive indexes) so that light will be able to cross the tissue more uniformly. There are two techniques for tissue clearing: *Spalteholtz's* method of solvent-based tissue dehydration and the aqueous-based techniques. The first technique dehydrates the tissue and removes lipids. Afterwards, the tissue is placed in higher refractive index solution that removes lipids and clears the tissue. One example is the iDISCO technique[39]. The aqueous-based techniques emerged due to loss of fluorescence from endogenous fluorescence proteins (eg GFP or lipophilic dyes) [38]. There are three approaches to aqueous-based which are simple immersion (ClearT2[40]), hyperhydration (Scale[41] and CUBIC[42,43]) and hydrogel embedding (PACT[44]). Some of these techniques, despite preserving fluorescence, take a long time to acquire the transparency in larger tissues, not to mention that they use highly denaturing agents to which some antibodies are sensitive[45,38]. In this thesis we focus on establishing a protocol that clears and allows the specific vessel markers staining compatibility in order to acquire large 3D images for polarity analysis.

Chapter II – Materials and Methods

II.1. Mice manipulation and Perfusion

All mice used during this project were sacrificed using CO_2 exposure. All animals were fed freely and housed in SPF facilities. Animal experiments were approved by the Animal Ethics Committee of Instituto de Medicina Molecular (iMM) and according to National Regulations.

II.1.1. Simple perfusion protocol

A needle was inserted in the left ventricle to perfuse the reagents. The collecting product would exit the vasculature through an induced lesion in the right atrium. The first reagent perfused was PBS 1x (pH7.4) with Heparin (10U/mL) to clear the blood. Afterwards, organs were fixed in 4% (wt/v) PFA in PBS 1x solution in order to preserve the vascular architecture and finally washed in PBS 1x (pH7.4). The organs were removed and immersed in a 4% (wt/v) PFA solution for post fixation overnight in a roller at 4°C[44].

II.1.2. CUBIC - CB-perfusion

After perfusion of PBS/Heparin (10U/mL), 4%PFA and PBS 1x, 30 mL of a ½ diluted Reagent 1/water solution was perfused. After acquiring a translucid appearance, the organs were removed and directly placed in Reagent 1 overnight at 37°C shaking. Reagent 1 was being replaced as the solution would turn green, from heme solubilization, for 3 days at 37°C shaking. To stop the clearing with reagent 1, the organs were washed with PBS (3x 2h). After the immunostaining the organs were placed in 50% Glycerol solution overnight and then placed in Reagent 2 for clearing (final refractive index matching). The following day the Reagent 2 was replaced. Reagents formulation in Supplementary Table 2 and were prepared according to the described protocol[46] – a modified version of this protocol is described below in clearing techniques.

II.1.3. Modified CUBIC

After perfusion of PBS/Heparin (10U/mL), 4%PFA and PBS 1x, 20 mL of a ½ diluted Reagent 1/water solution was perfused and then washed out with PBS 1x. Extracted organs were post fixed with 4%PFA overnight at 4°C. After PBS 1x washes the organs were immersed in Reagent 1 for one day. After PBS 1x washes, immunostaining was performed and then a post-fixation step was conducted. Afterwards organs were placed in 50% Glycerol solution overnight. The following day the tissues were immersed in Reagent2.

II.2. Immunostaining Protocol

II.2.1. Organs

The organs were immersed in a pre-treatment solution (formulation in Supplementary Table 2) overnight, followed by CBB (Cláudio's blocking buffer) (formulation in Supplementary Table 2) washes every 2h and overnight. Samples were incubated with the primary antibodies (1:200 Rat anti-ICAM and Rabbit anti-Erg in 1:1 PBS/CBB) for two days. The organs were washed with PBT solution (0,1%Triton X-100 in PBS 1x) with 2h washes over the course of a day and overnight. Then, samples were incubated in secondary antibody solution (1:200 IgG anti-Rat conjugated with AlexaFluor 555 and IgG anti-rabbit conjugated with AlexaFluor 647 in 1:1 PBS/CBB) for two days. Afterwards, the organs were washed with PBT and further stored in PBT.

II.2.2. Retinas

Pre-treatment was applied for 4h/overnight at 4^{o}C with shaking. Afterwards, retinas were incubated in 100µL of primary antibody solution (1:200 Rat anti-ICAM and 1:400 Rabbit anti-Erg in 1:1 PBS/CBB) overnight at 4^{o}C, washed with PBT 3x60min and then incubated in 100µL of secondary antibody solution (1:200 IgG anti-Rat conjugated with AlexaFluor 555 and 1:400 IgG anti-rabbit conjugated with AlexaFluor 647), 4^{o}C overnight. These retinas were washed afterwards with PBT and stored in PBT at 4^{o}C.

II.2.3. GOLGI immunostaining in organs

Because golgi and nucleus primary antibodies were raised in the same species the immunostaining protocol was different. The organs were immersed in a pre-treatment solution overnight, followed by CBB washes every 2h and overnight. Samples were then incubated with the primary antibodies (1:200 Rat anti-ICAM and Rabbit anti-GOLPH4 in 1:1 PBS/CBB) for two days, washed with PBT every 2h and overnight and then incubated with a secondary antibody solution (1:200 IgG anti-Rat conjugated with AlexaFluor 555 and IgG anti-rabbit conjugated with AlexaFluor 488 in 1:1 PBS/CBB). After PBT washes, organs were incubated with anti-rabbit Fab fragments to block the anti-GOLPH4 primary antibodies and this blocking was fixed with 4%PFA for 15 min. After PBS 1x washes, organs were incubated in CBB overnight and then incubated with rabbit anti-ERG 1:200 in PBS/CBB. After PBT washes, secondary antibody incubation started using IgG anti-rabbit conjugated with AlexaFluor 647 in 1:1 PBS/CBB. Afterwards, organs were post fixed with 4%PFA/1%Glutaraldehyde overnight at 4^{o}C.

II.3. Clearing Techniques

II.3.1. ClearT2 Protocol

Following immunostaining, organs were placed in a 25%Formamide/10%PEG solution for 1h. Next, samples were immersed in a 50%Formamide/20%PEG solution for 1h, and the solution replaced for another 16h. Samples were immediately imaged using the final clearing solution as imaging solution. The clearing solutions were prepared according to the described protocol[40]

II.3.2. iDISCO Protocol

Samples were washed with 0,2%Triton X-100 in PBS 1x and immersed in PBS/0.2% TritonX-100/20% DMSO, at 37°C overnight. Then, samples were immersed in PBS/0.1% Tween-20/0.1% Triton X- 100/0.1% deoxycholate/0.1% NP40/20% DMSO, at 37°C overnight and washed in 0,2%Triton X-100 in PBS 1x. Then they were immersed in PBS/0.2% Triton X-100/20% DMSO/ 0.3 M glycine at 37°C overnight and in PBS/0.2% Triton X-100/ 10% DMSO/6%FBS at 37°C overnight. Immunostaining was performed as described before. The clearing starts with an overnight incubation of the samples in 50% v/v tetrahydrofuran/H2O (THF) in a glass vial with a silicon-coated cap. Afterwards samples were immersed in 80% THF/H_2O for 1 hr and 100% THF for 1h twice. Samples were then dried and placed in dichloromethane (DCM) until they sank at the bottom of the vial. Finally, samples were placed in dibenzyl ether (DBE) until clearing was achieved.

II.3.3. PACT Protocol

After post fixation in PFA, samples were Incubated in monomer A4P0 (Acrylamide 4%, PFA 0%) supplemented with photoinitiator 2,2'-Azobis[2-(2-imidazolin-2-yl)propane] dihydrochloride 0,25% at 4°C overnight. Then they were transferred to a 37°C waterbath for 6h for polymerization. Samples were incubated in 8%SDS solution at 37°C shaking for 2-5 days. The immunostaining was performed after clearing and afterwards samples were placed in Imaging media RIMS (88% Histodenz in water).

II.3.4. Protocol 1

Part of the CB-perfusion was performed, applying the perfusion of PBS/Heparin (10U/mL), 4% PFA and diluted Reagent1, but, afterwards, Reagent1 was cleared out with PBS1x and the organs were extracted for post fixation overnight at 4°C. Then immunostaining was performed and clearing performed with ClearT2.

II.3.5. Protocol2 – Second Modified CB-perfusion

After perfusion of diluted Reagent 1, PBS1x was perfused to clear out the Reagent1 and organs were extracted for post fixation overnight at 4°C. Then immunostaining was performed. After

post fixation of the immunostaining, organs were immersed in Reagent1 only for 1day, washed out with PBS1x, immersed in 50%Glycerol for overnight and placed in Reagent2 for two days.

II.4. Imaging

Image acquisition was made using Point Scanning Confocal microscopes Zeiss LSM 710, LSM 880 and Light Sheet Fluorescence microscope Zeiss Lightsheet Z1. Samples were first evaluated with the confocal microscopes for signal strength using fluorodishes. The last clearing solution was used to cover the bottom of the dish and the organs were placed in the dish. Afterwards, organs were imaged in sRIMS/RIMS solution, the solution with compatible RI and the one solution to be used in the Lightsheet chamber. After checking signal quality with confocal microscopes, the samples that were most cleared were visualized with the lightsheet. The lightsheet microscope has a chamber that is filled with the imaging media with RI matching the tissues. The tissues were glued to a capillary and placed inside the chamber. The capillary was controlled by the software in order to position the sample in terms of xyz coordinates inside the chamber and the angle that allows the lightsheet to pass. The imaging software used was Zeiss Zen lite® that supports CZI formats.

II.5. Processing

Images from confocal acquisition were processed by image analysis and visualization software Fiji. In Fiji, the z-stacks were downsampled by Maximum Intensity Projection (MIP) to a single image in order to adjust signal brightness and contrast. After processing, files were converted to TIFF format. CZI files can also be directly opened on Imaris® which is a 3D and 4D real time interactive data visualization and management software. Lightsheet images were processed on Arivis 4D Vision® for images that were acquired using multiview combined with tile scan mode. Arivis 4D vision® is the software that allows handling of huge amount of multi-channel data. It provides tools for stitching and alignment to generated multidimensional image stacks Because Arivis generates files with SIS format, not recognizable by Imaris®, after processing with Arivis software for stitching, the image was converted to TIFF, generating a number of TIFF files equal to the number of Z-stacks and with separated channels. Using Fiji, the files were assembled for each channel, then merged and a Hyperstack was created. On Imaris® we could open these TIFF files. For images that were acquired with a simple Z-stack on lightsheet, the files could be directly opened on Imaris.

II.6. Polarity vectors drawing

Using Fiji each channel was saved separately. They were assembled and saved in TIFF format. Using a Matlab script designed for polarity analysis in 2D images, the image was opened and the vectors were drawn from nucleus to Golgi. Because Golgi staining is not specific for EC, we had to maintain an opened file with separated Z-stack in order to detect which Golgi belonged to which nuclei.

Chapter III: Results

III.Clearing Techniques

The vascular network visualization in organs requires the application of clearing techniques and immunofluorescence in order to enable us to visualize vessel lumen (stained with anti-ICAM2/CD102), endothelial nuclei (stained with anti-ERG - erythroblast transformation-specific-related gene) and the Golgi apparatus (stained with anti-GOLPH4). These clearing techniques were optimized for imaging with lightsheet microscopy. In a first approach, we selected four clearing methods according to the previews descriptions of each technique, immunostaining compatibility and fluorophore emission[38]. Due to the fact that ICAM2 binds to the vessel membrane, we considered that techniques of passive delipidation would interfere with that specific staining. However previous descriptions showed compatibility of some of these clearing techniques (iDISCO, PACT and CUBIC) with membrane staining. We decided to begin testing the clearing methods with iDISCO (a basic technique belonging to the solvent-based clearing approach), ClearT2 (a simple immersion approach that uses formamide), PACT (an improved technique from the hydrogel-embedding approach) and CUBIC (an Hyperhydration approach) (see Table 1 for details).

iDISCO - immunolabelling-enabled three-dimensional imaging of solvent-cleared organs

The Solvent-based clearing techniques were the first to be developed. For more than one century resins were used in the biology field to stabilize samples, because of their hydrophobicity that would cause dehydration of tissue. *Spalteholz* first described a clearing method for large tissue in the beginning of the 20th century, but it was a harsh method that would damage the surface few centimeters. For solvent-based clearing techniques the first step is tissue dehydration, since water holds a lower refractive index compared to cellular structures. Tissues are immersed in alcohol/water solutions (with progressive decrease of water concentration), followed by immersion in solvents that delipidize the tissue[45].

ClearT2

ClearT2 is a simple immersion technique that does not remove lipids or water. It is an improvement of ClearT technique in which formamide is used to better match the refractive index of tissues. But formamide alone was not compatible with immunostaining or fluorophore emission, so ClearT2 was developed by adding Polyethilene Glycol (PEG) to the formamide solution. PEG would help to stabilize the protein conformation as well as immunostaining and fluorophore emission[40].

PACT - passive clarity technique

PACT is a hydrogel embedding technique in which the hydrogel is used for purpose of tissue structure stability, lipids are then extracted with ionic detergents and finally the cleared tissue is

embedded in an imaging solution designated RIMS (Refractive index matching solution) that has a RI range from 1.38–1.48, depending on the concentration of the Histodenz in the RIMS solution. Based on CLARITY clearing, which introduced the crosslink and hydrogel-monomer hybridization and used ETC (electrophoretic tissue clearing), PACT uses a softer technique of clearing. The adjustments made started with the use of Acrylamid rather than BisAcrylamide as monomers for hydrogel polymerization. ETC was a faster method of removing lipids than passive delipidation with large micelle, but tissues would degrade more so 8%SDS was used to clear large tissues[44].

CUBIC - Clear, Unobstructed Brain Imaging Cocktails and Computational analysis

CUBIC is an hyperhydration technique that was developed from Scale, which uses Glycerol, Urea and Triton X-100 to clear the tissue. CUBIC was developed through a chemical screening of the Scale solutions. The first screening pointed to aminoalcohols ability to solubilize tissue. In the second screening the cocktail (Reagent1), composed of N,N,N',N'-tetrakis(2-hydroxypropyl)ethylenediamine (designated aminoalcohol #10), Triton and Urea was chosen. This reagent would passively remove the lipids and also decolorize the tissue (a property of aminoalcohol #10 to release the heme from hemoglobin), but the RI of the cleared tissue and of the solution were mismatched. A third screening created the Reagent2, which is a modification of Reagent1 recipe, by adding Sucrose, instead of Glycerol, in order to increase the solution RI and substitute aminoalcohol #10 by 2,2',2''-nitrilotriethanol (#16). This reagent would enhance optical clearance of the delipidized tissue. The effect of hyperhydration is caused by urea which is responsible for expanding the tissue through an osmotic gradient that causes water to be pulled into regions of tightly folded regions in proteins, causing them to hydrate, expand and decrease their refractive index. CUBIC has tree protocols to apply. The simple immersion protocol consists in clearing only by immersion of tissues in the

Table 1 Description of the Clearing Techniques

		Clearing solutions	Imaging Solution	RI	Steps			
Solvent-Based technique								
	iDISCO	DCM and DBE	DBE	1.56	Immunostaining	Dehydration	Delipidation	
Aqueous Based clearing technique								
Simple Immersion	**ClearT2**	Formamide/ PEG	Formamide/ PEG	1.44	Immunostaining	Formamide Immersion	sRIMS	
Hydrogel embedding	**PACT**	8%SDS	RIMS	1.46	Hydrogel Hybridization	8%SDS clearing	Immunostaining	RIMS
Hyperhydration	**CUBIC**	Reagent1/ Reagent2	RIMS	1.48	Reagent 1	Immunostaining	Reagent2	RIMS

DCM , Dichloromethane; DBE, Dibenzylther; PEG, Polyethilene Glycol; RIMS, Refractive índex match solution made with histodenz; sRIMS, RIMS made with sorbitol; The CUBIC technique was CB-perfusion that starts with perfusion of diluted Reagent1. Details of Reagents and Refractive indexes in Supplementay Tables 2 and 5

Reagents. The second protocol, more efficient, is designated CB-perfusion and starts with diluted Reagent 1 in the perfusion and immersion of tissues in the Reagents. This protocol clears the tissues better than the original protocol. The third protocol is called Whole-body perfusion in which all Reagents are perfused and the entire body of the mouse turns transparent. The CUBIC protocol that we used was the CB-perfusion protocol[42,46].

III.1. Blood Vessel Visualization

III.1.1. Testing Clearing Techniques

To begin visualizing organs, we started using pups due to their small size. The procedure started with perfusion of the mouse to clear blood and to fixate the structures (especially the vascular pattern). The iDISCO, ClearT2 and PACT techniques started with a simple perfusion, whereas CUBIC started with a more complex perfusion of ½ diluted Reagent1 (CB-perfusion). Afterwards, kidney, intestine and liver were extracted, stained for ICAM-2 and ERG only and further cleared applying the described clearing techniques (Table 1 and Supplementary Table 1).

The vessel lumen staining (with anti-ICAM2) was sensitive to delipidation-based techniques, since the vessel staining was weak in iDISCO, PACT and CUBIC techniques, even though they had the best tissue clearing (Figure 5). iDISCO technique was excluded since it was not compatible with ICAM-2 and ERG stainings (Figure 5). ClearT2 had the best immunostaining compatibility (Figure 5). In this technique the clearing of the analyzed organs was weaker but, because it does not remove

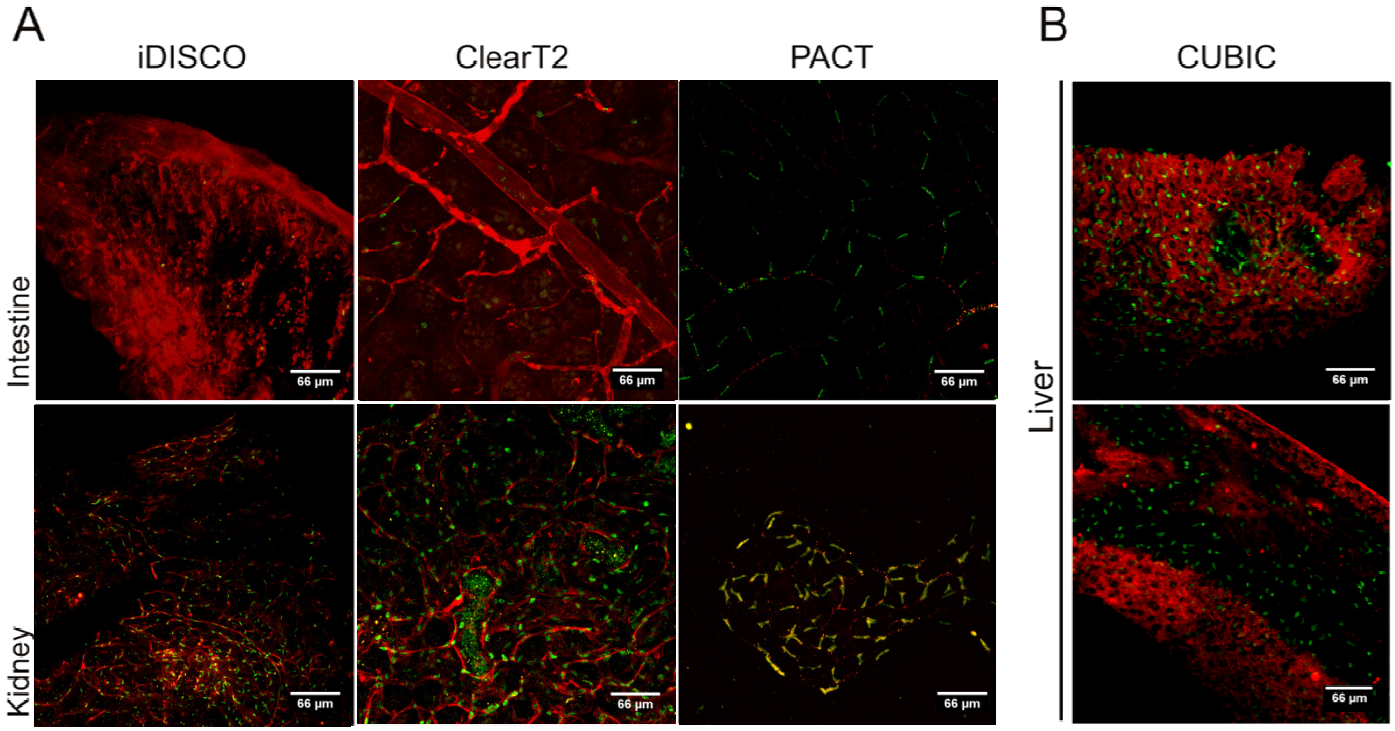

Figure 5 - Test of different clearing techniques. The first try of clearing techniques used intestine and kidney stained with anti-Erg for nucleus (in green) and anti-ICAM-2 for vessel lumen (in red) and visualized in confocal with 20x objective. The clearing techniques applied were solvent-based clearing iDISCO, aqueous based techniques ClearT2 (simple immersion) and PACT (hydrogel embedding). ClearT2 shows better immunostaining compatibility in both organs. The test of aqueous-based technique of hyperhydration CUBIC used only liver. The clearing efficiency of CUBIC is very good, but it is not compatible with ICAM staining. All images are MIP of 13 to 42 z-stacks. Thickness of tissues is on Supplementary Table 3.

lipids, the staining with anti-ICAM2 and anti-ERG was good (Figure 5). Indeed, ClearT2 showed us good results compared to the other techniques, but clearing becomes extremely limited when working with thicker and denser tissues (such as the liver). PACT and CUBIC had the best clearing results, but either ICAM-2 staining was not present or the signal was very weak (Figure 5). CUBIC technique was used specifically for the liver, the hardest organ to stain and clearing (Figure 1). However, the ICAM-2 staining compatibility was similar to PACT protocol. ERG staining was present in most of the applied techniques. These data point out to the need of combine and optimize different clearing and immunostaining techniques in order to achieve a clear and immunostained organ, so we started optimizing these protocols.

III.1.2. Optimization

Due to the need of an optimization of the applied techniques we first decided to separate the PACT steps of hydrogel polymerization (A4P0) and 8% SDS clearing to see which step was damaging the vascular membranes (ICAM-2 staining). Additionally, we tested a pre-treatment solution applied to the organs to test if the staining could be improved by better antibody penetration (Figure 6 and supplementary Table 2). This pre-treatment solution was based on the blocking buffer, but with additional reagents to increase antibody penetration, such as Tween20 and NP40 that are detergents that efficiently solubilise the membrane without dissolving it. Also the presence of urea in the pre-treatment showed improved signal (Supplementary Figure 1). We also tested if switching the immunostaining with the 8% SDS clearing (by performing the staining first) could, perhaps, help in the preservation of the ICAM-2 staining. ClearT2 was the clearing technique applied to all these conditions, except for the ones that were cleared by 8% SDS, because ClearT2 was previously shown to be the best immunostaining compatible clearing technique (Figure 5).

Pre-treatment usage showed an improved signal in the analysed organs, even better than the CleartT2 protocol, used as a control, (Figure 6A and 6B). Switching the steps of immunostaining and 8% SDS slightly increased immunostaining compatibility, but the structures could not be entirely visualized due to the signal weakness with depth of the organ (Figure 6C and 6D). Using Hydrogel hybridization (A4P0) to stabilize the tissue and applying ClearT2 clearing revealed severe quenching of fluorescence (Figure 6E). Both steps of PACT, 8% SDS clearing and hydrogel hybridization (A4P0), compromise staining compatibility, so we decided to stop using these techniques (Figure 6C to 6E). Liver has showed complications for staining and clearing in the various techniques, it is an extremely difficult organ to clear. This showed us that PACT is not the best technique to be used and that the pre-treatment step is crucial for a good antibody penetration and, consequently, a good immunostaining coupled with clearing. The pre-treatment step was, afterwards, used in all the experiments. Through the course of the experiments we found that in order to obtain the best

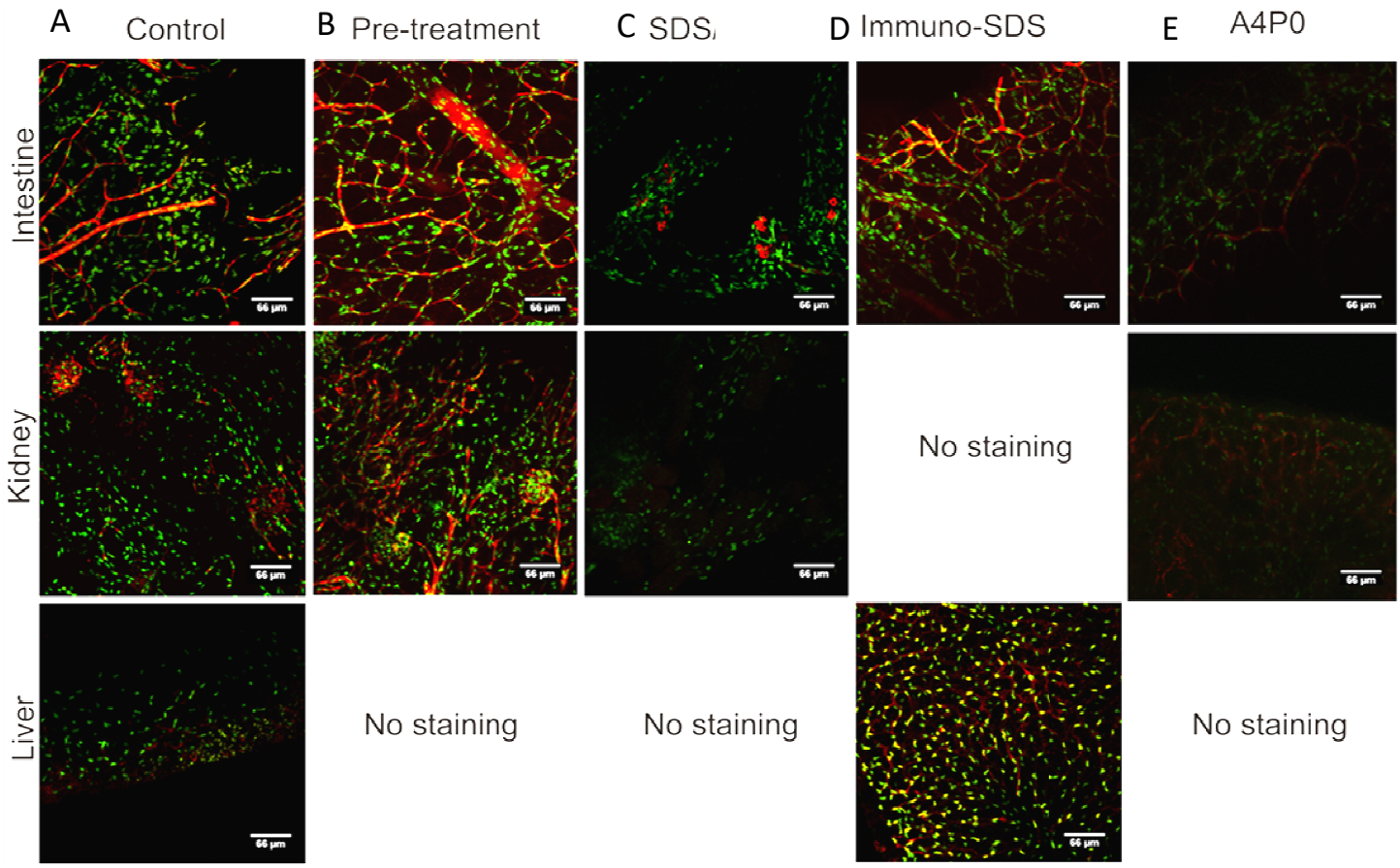

Figure 6 - Clearing Techniques optimization. A) the Control is the clearing Technique of ClearT2. B) is the addition of a Pre-treatment step prior to CBB blocking. C) is the clearing of the samples by 8%SDS solution for short time, followed by immunostaining. D) is the switch of the 8%SDS clearing and immunostaining steps, in which immunostaining came before 8%SDS clearing. E) is the polymerization of samples with 4%Acrylamide solution, immunostained and cleared by Formamide. Pre-treatment showed better results in terms of signal and antibody penetration, better than control. Protocols that included 8%SDS were not immunostaining compatible. Even though switching the SDS and immunostaining steps had better result, it was not good enough. A4P0 completely quenched the fluorescence. All images are MIP of 12 to 24 z-stacks. See supplementary Table 3.

cleared organs, no matter what clearing technique is being applied, is having the best perfusion possible, because blood interferes with clearing efficiency (Supplementary Figure 2). The best way to control a good perfusion is through the liver, which is the most visible organ when opening the mouse. The liver will turn very clear almost immediately, if the perfusion is being done correctly.

We also optimized the CUBIC technique during the test of different protocols (described below).

III.1.2.1. Other protocols

Over the course of experiments, we observed that organs seem to have different compatibilities with the different clearing protocols, so we decided to test three protocols (please see Supplementary Table 1) for brain, kidney and intestine, the easiest organs to handle during the different protocols. We used ClearT2 as the control protocol and we also used the CUBIC protocol but with a modification (a post fixation step after perfusion). The other protocols tested were Protocol 1 (a mix of the diluted Reagent 1 perfusion (designated CB perfusion) with ClearT2) and Protocol 2 (a modified version of CUBIC in which, in addition to post fixation, the immunostaining

would be performed first, then fixated again and the clearing would be performed after). We wanted to see if the perfusion of ½ diluted Reagent 1 would enhance the final clearing and if it would interfere with the staining regardless of the clearing technique applied (Control against Protocol 1). Also, we wanted to see if the switching of the steps of Reagent 1 with immunostaining would improve the staining (CUBIC against Protocol 2). Our results show that perfusion of diluted Reagent 1 does not perturb the immunostaining, instead, it seems to improve the signal, as more defined structures with increased signal penetration and less background were observed (as seen for the intestine in Figure 7). Furthermore, this protocol increased the final clearing obtained by ClearT2 (Figure 7 and Supplementary Figure 2). Nevertheless, the final clearing of the organs was not good enough for imaging in the light-sheet microscope, especially for the kidney.

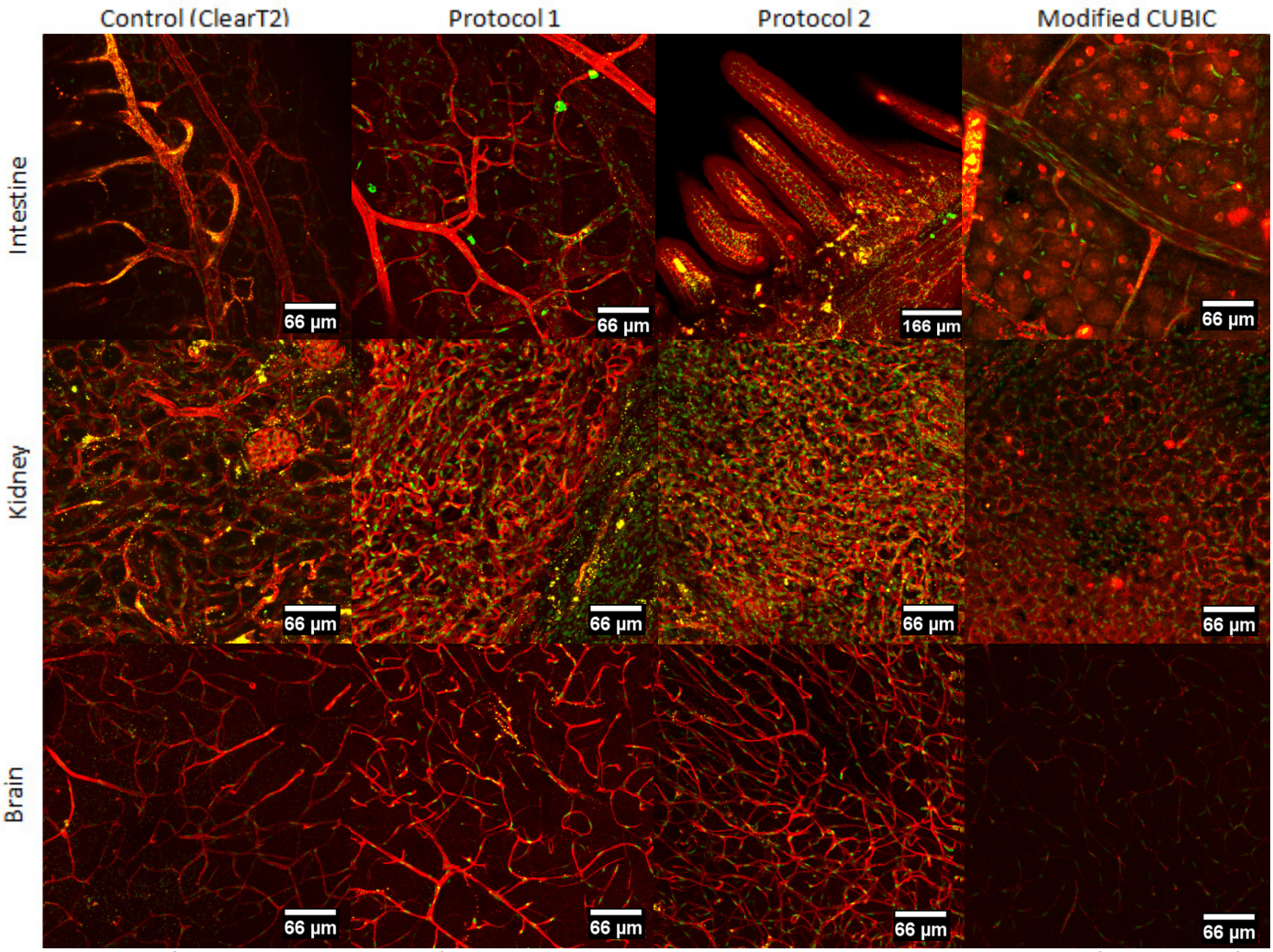

Figure 7 - Test of other clearing protocols for intestine, kidney and brain. All protocols started with a modified version of CB-perfusion, except for control that started with a simple perfusion. Control is the original technique of ClearT2 tested in section 1.1. Protocol1 is the improved protocol of ClearT2 which mixes the perfusion of CUBIC technique with the clearing of Cleart2. Protocol2 is a modified protocol of CUBIC that has more steps of post fixation and switches the steps of immunostaining with the clearing with Reagent1. CUBIC is the modification of the original protocols in which the perfusion of diluted Reagent1 is followed by post-fixation overnight with 4%PFA. Results point to Protocol2 being the most suitable protocol to be used in the following experiments as the signal seems to be the best. It seems that intestine has better signal using Protocol 1 and brain and kidney are better with Protocol 2. All images are MIP. The z-stacks acquired for Modified CUBIC were between 17 to 37 z-stacks, due to lack of signal. The other three protocols had 64 to 177 z-stacks. See supplementary Table 3.

Regarding the switching of Reagent 1 with immunostaining, our results show that performing the immunostaining before clearing with Reagent 1 and 2 (Protocol2) improved the immunostaining signal when comparing with the original protocol and even the modified version of CUBIC. The level of transparency and signal obtained were better in Protocol 2 compared to the control, and even to Protocol 1 (which is an improvement of the control). Taking in consideration the compromise between the signal obtained and the level of transparency acquired, it is clear that Protocol 2 was the best protocol to be applied in the polarity assessment of organ vasculature.

III.1.3. Golgi staining with GOLPH4

After testing and optimizing the clearing protocols for nucleus and vessel lumen, the final staining of the golgi was added to the immunostaining protocol and the clearing with Protocol2 was applied. The staining worked and was compatible with the clearing protocol (Figure 8). The protocol of immunostaining was extended since anti-ERG and anti-GOLPH4 antibodies were raised in the same species and so there is high cross reaction between the secondary antibodies. In the acquired images (Figure 8), we observe, on the merged channels' image, mainly the ERG and ICAM2 signals. Golgi is present, only it's masked by the signal in the 647 channel (the ERG channel), because golgi was stained first, together with anti-ICAM2, and ERG was stained separately from these afterwards, and so the secondary antibody cross reacted with anti-GOLPH4. After checking the presence of the

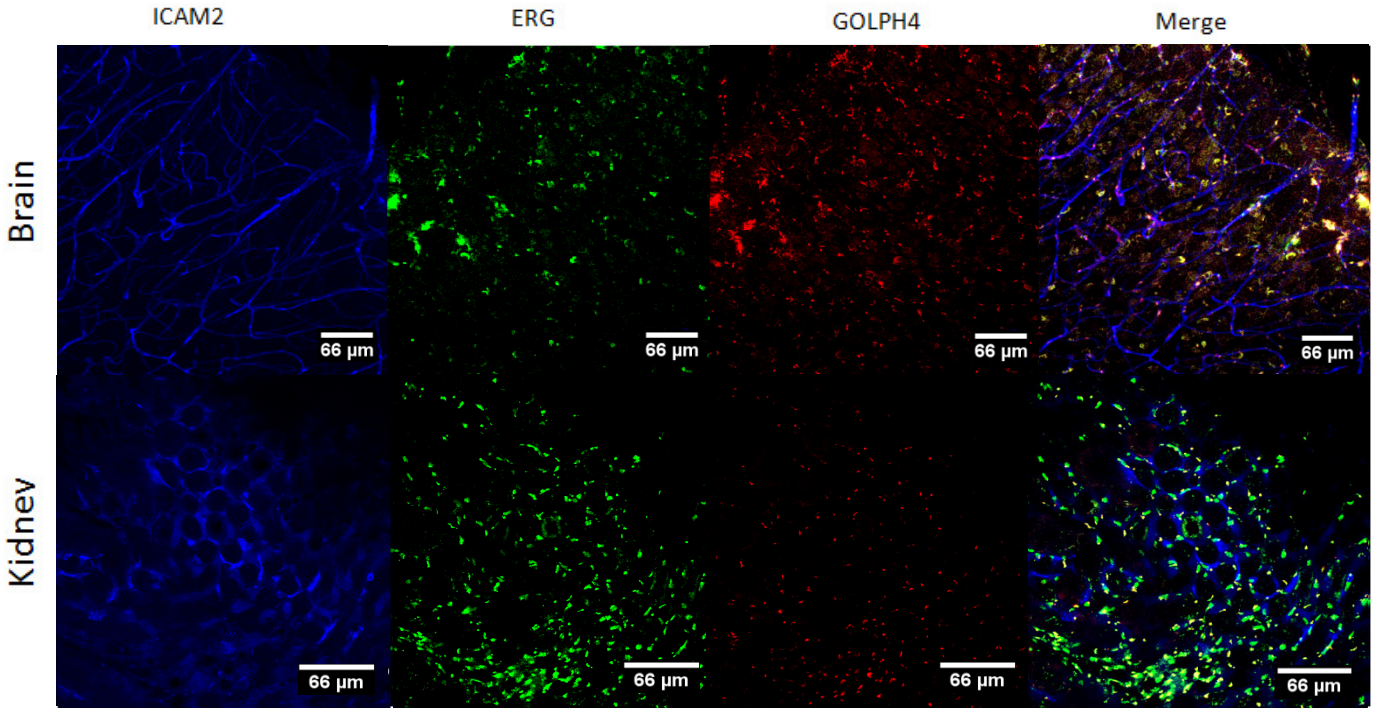

Figure 8 - Protocol 2 applied to triple immunostaining of the brain and kidney. In blue is the vessel lumen staining for ICAM2, in green is the nucleus staining for ERG and in red is the golgi staining for GOLPH4. There is cross reaction between the GOLPH4 and ERG staining. ERG staining was performed last so the channel in green has nucleus and golgi. The merge images have the golgi 488 signal masked by the signal captured in the 647 channel. Images are MIP of 5 z-stacks (for kidney) and 60 z-Stacks (for brain). See supplementary Table 3.

three stainings in the confocal, the tissues were taken to the lightsheet for large 3D acquisition (data not shown). For the images that were acquired, these needed to be treated in order to distinguish the nucleus and golgi signal and proceed to polarity assessment. The image treatment is discussed further ahead in the Polarity assessment section.

III.2. Imaging with Light-sheet

For 3D visualization we used lightsheet microscopy. Light-sheet fluorescence microscopy (LSFM) functions as a microscope and a non-destructive microtome, since it allows deep imaging using thin planes of light to optically section transparent samples that have been labelled. It allows fast and resolved images with minimized photobleaching or phototoxicity due to a more efficient illumination and light detection setup[47]. The instrument part that allows this type of imaging consists in two side objectives, which work as light condensers, that are positioned one in front of the other to allow dual-side illumination of the tissue in order to eliminate shadow artefacts and increase intensity and homogeneity of illumination (Figure 9). A detection objective is positioned orthogonally to capture the fluorescence. The positioning of the two side objectives and detection objective is what allows the optical sectioning with minimal photodamage, since the light is illuminating only that plane without crossing the entire sample. The sample is placed inside a chamber filled with the imaging media. The detection objective (special immersion objective) seals the chamber by being immersed in the media to reduce air/media RI mismatches (only the illuminators are placed in air). The acquisition computer sends information directly to a processing computer with the software required for ultamicroscopy processing.

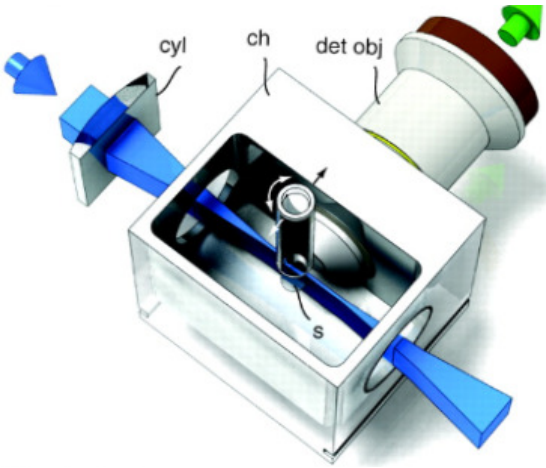

Figure 9 - Light-sheet microscopy. The sample is placed inside a chamber filled with imaging media (ch). Two cylindrical objectives (cyl), also called illuminators, illuminate the sample with a thin light sheet that allows optical sectioning of the transparent tissue. The fluorescence is detected by a detection objective (det obj) that projects the fluorescence light on to a camera[65].

To optimize the light-sheet microscope before using it in the acquisition of larger cleared organs, we used retinas due to their small size and natural transparency (no need to apply clearing techniques). Some settings were tested to see if we could fasten the acquisition without losing too much resolution, since our samples were big and the data generated was larger (Supplementary Figure 3).

III.2.1. Retinas imaging

The first retina analysed was acquired with incomplete data, since the whole organ would create around 2Tb of raw data that would become almost impossible to process. To fasten the acquisition and decrease the amount of data, only part of the retina was acquired. A small Z-stack was defined with 4x the optimal interval recommended. The retina was acquired with 20x clearing immersion objective and with tile scan mode that defines a tile grid that allows scanning of larger areas. After the acquisition, Arivis software was used to perform stitching of the tiles (Figure10A), and then the data was transferred to Imaris software. Both Arivis and Imaris were used to compare the quality of rendering and visualization of vessels and organelles (Figure 10 and supplementary

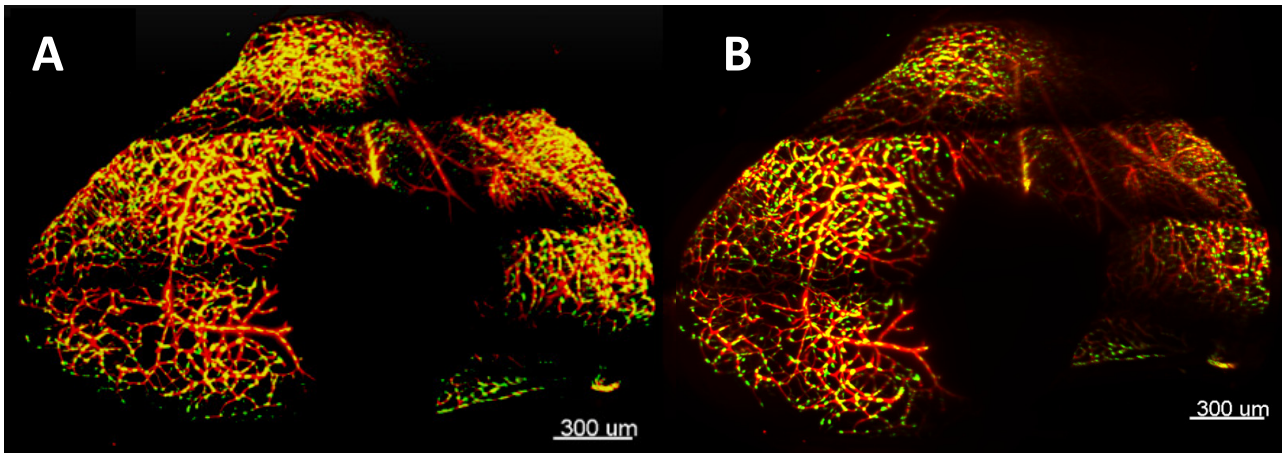

Figure 10.Test of light-sheet acquired retina. A) is the retina processed with Arivis. B) is the same retina visualized with Imaris. Both have good rendering capacity, but for real-time manipulation of images, Imaris is better.

Figure 3A). Next the same retina was fully imaged, but the signal was less intense than the first time (Supplementary Figure 3B). Both 3D reconstructions of the retinas show stripes correspondent to the Y axis tile grid (the fluorescence captured on the bottom of each tile is decreased). This effect repeated itself through several retina acquisitions, and so we believed that these stripes had to do with a problem in the acquisition in tile mode itself and not a problem from the samples. In the following acquisitions we acquired with more than 30% overlapping tiles to see if this effect disappeared and it did (Supplementary Figure 3C - only half a retina was acquired in this test due to a huge amount of data from acquiring a whole retina). Even with a 40% overlapping setting, the algorithms provided by Arivis weren't able to correctly align the tiles, so these were aligned manually. The manual alignment can be accurate since common structures can be visualized in different tiles and it becomes easy to overlap them manually.

III.2.2. Organ Imaging

After testing the system with retinas, we decided to start testing the cleared organs. Each organ was first observed at a confocal microscope for signal checking and only after, depending on

the strength of signal and level of transparency, would they be visualized at the lightsheet microscope.

We first attempted to acquire brain tissue (Supplementary Figure 3D), as it was the most cleared tissue with a very simple vascular network with good signal. The same brain tissue was imaged in confocal, using a 20x objective, and we acquired an image around 0,162 mm whereas with the light-sheet (using a clearing 20x objective) we obtained a 0,483 mm thick image (Figure 11). The signal is more resolved in the confocal, than in light-sheet, and it seems to have less signal decay, but the thickness acquired was less than half of the thickness acquired in light-sheet; any deeper and the signal would equally start to decay. In the light-sheet acquired image, we selected the region with good signal, until it starts to decay, and this section has a thickness of 0,200 mm, which is close to the confocal acquired thickness (Figure 11). The confocal microscopy provides more resolved images, but the working distance of the objectives is quite limiting, not being so helpful for large 3D reconstruction (Supplementary Table 4). Confocal 10x dry objective has a working distance close to that of the 20x clearing in the lightsheet, but spherical aberration compromises resolution in depth and makes it hard to analyse the images in which we need to distinguish nucleus and golgi. As for light-sheet, the resolution can be increased by altering the settings of acquisition mode (in this case we acquired in Z-stack without continuous drive mode, which is a faster mode that lessens the resolution – see Supplementary Figure 4) and by using a multiview mode that allows to image the same region from different angles, compensating for signal decay (data not shown).

Confocal is a good choice for acquiring small sections of tissues, providing a good resolved image, but the use of lightsheet for large 3D reconstruction is recommended. If the tissue is very well cleared the signal is easily captured from both sides and a better image of the whole tissue can be acquired compared to the confocal.

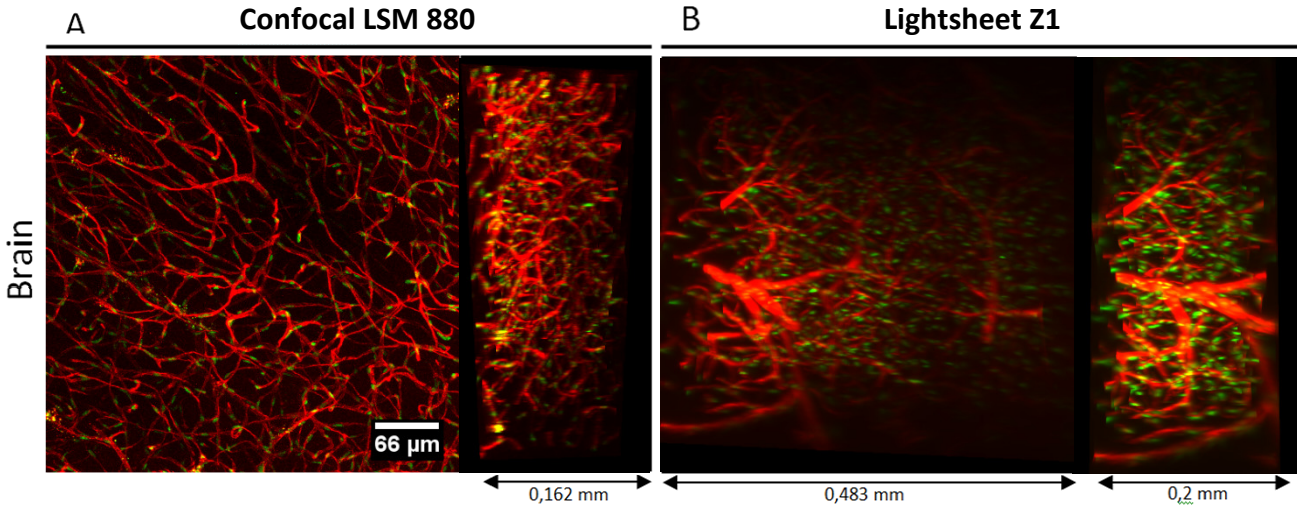

Figure 11 - Confocal and Lightsheet Brain acquisition. The same Brain tissue was visualized in A) the Confocal LSM 880 and B) in the lightsheet. Both images are snapshots from Imaris. In A) we have a frontal (MIP) and lateral view of the Z-stack acquired image. In B) we have both lateral views for lightsheet acquired image. The first is the whole Z-stack acquired that has 0,483mm and the second is the cropped Z-stack that has 0,2mm.

Regarding other organs, kidney has a very dense vascular network and its functional unit, the glomeruli, is very difficult to resolve in either the confocal or lightsheet. Using 40x objective in confocal we were able to acquire a small Z-stack of the network for polarity assays, but the glomeruli, which is a very important structure to acquire, needs further improvement in acquisition settings. As for intestine, confocal microscopy provides the essential for polarity analysis. The villi, the intestine-specific structure, can easily be acquired using just the confocal microscopy.

III.3. Polarity assessment in Organs' vasculature

To assess the polarity of cells, two major organelles are necessary to define the orientation of the cell (nucleus and golgi). In Franco et al. polarity is defined as a vector with origin in the nucleus and pointing towards the golgi [21]. The direction of the vector gives insights of polarization of the endothelial cell and, consequently, direction of migration. Using a Matlab script designed specifically for polarity vector drawing, we were able to draw the vectors in the acquired images (Figure 12). Unfortunately, the polarity analysis in organs is more complex than in retinas because the latter have a simple vascular network that can be approximated to a 2D network. The same cannot be done for organs, since they have a complex 3D network, so polarity analysis and flow simulations are not yet possible.

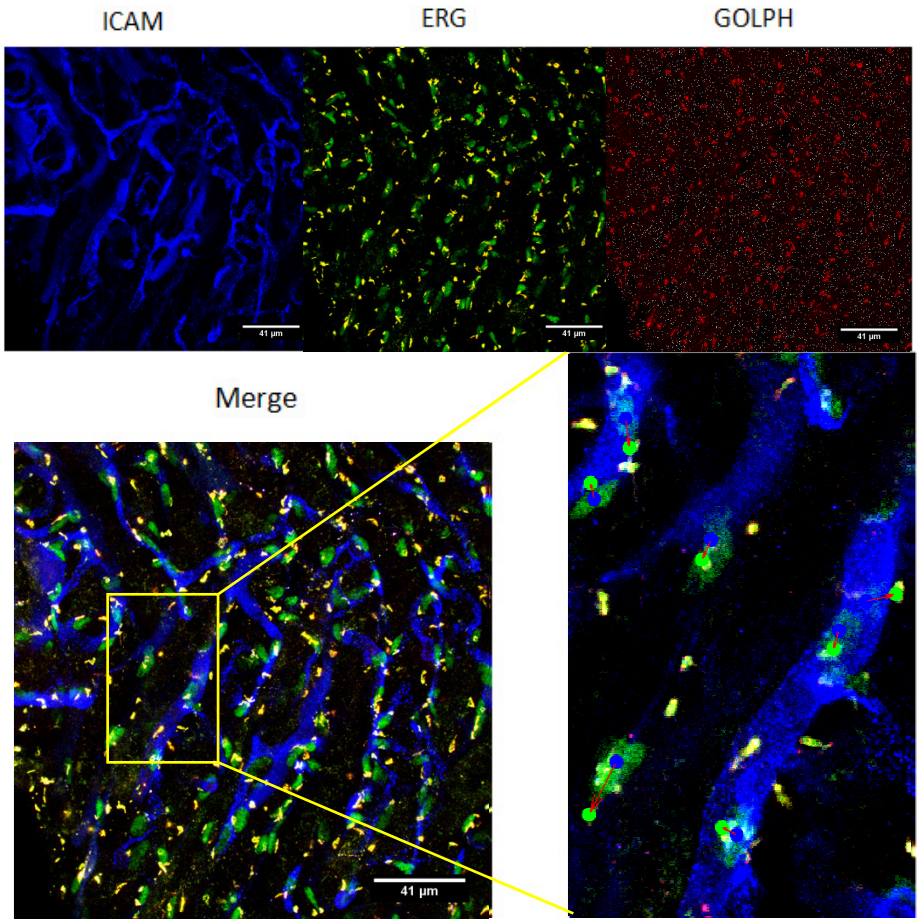

Figure 12.Polarity vector drawing in kidney. Using an image acquired in 40x objective of the kidney tissue, we proceeded to polarity vector drawing, using a MatLab script that was design specifically for polarity vectors in retina. Using an image with the separated Z-stack we were able to identify the nucleus and golgi from the same cell and draw vector from nucleus to golgi, defining the polarity of cells. This image is a MIP of 20 z-stacks. See supplementary Table 3

Chapter IV - Discussion

Studies in the mouse retina highlighted that VEGF regulates EC polarity in the plexus sprouting front, whereas shear stress is the driver of polarity in more distal areas of the plexus. These observations led us to propose the hypothesis that these two factors might compete with each other in order to establish the polarity of EC within the vascular network, and the sensitivity of ECs to this competitive mechanism could determine the outcome of vascular remodelling. Organs have intrinsic and different levels of VEGF and specialised vascular network connectivity. As such, the polarity response of ECs in these organ-specific microenvironments, arising from VEGF and flow regulation, could be one important determinant of organ-specific vascular networks. Therefore, the ability to analyse EC polarity patterns in whole organs could help understand the balance between the two drivers of EC polarity. Taking this in perspective, our main goal was to be able to visualize organ vascular patterns and to develop methods to analyse them.

IV.1. Deep Tissue Imaging

The issue of imaging thick tissues derives from light scattering. Multiple scattering consists of interference of scattered light from neighbor atoms and occurs laterally and forwardly. The consequence of this is the different light propagation speeds of each wavelength that are reflected in the refractive index of the media. The lateral scattering is the one that most interferes in imaging, since it causes translucence of tissues. So far the methods used for imaging consisted in sectioning the tissues, image them and perform 3D reconstruction. For 3D morphology understanding the final product of such approach is imperfect since sections tend to lose tissues, leading to loss of information, and distortion[38]. The treatment of sections for mounting tends to cause shrinkage of tissue, and the reconstructions come with scaling artifacts derived from shrinkage and refractive index mismatch (that alters axial dimension)[48]. Even though corrections can be made by adjusting the refractive index of media, by using methods that cause less distortion, using another numerical aperture (characteristic of each objective) and using computer methods for aiding the 3D reconstruction[49], the final volumetric reconstruction can be unsatisfactory.

The best way to perform 3D imaging of tissues is to use the whole tissue without physically sectioning it. And with the advent of optical-sectioning microscopes such as laser-scanning or spinning disk confocal microscopy, laser scanning two-photon microscopy and light-sheet microscopy, these could provide information of single planes, eliminating out-of-focus light. But still thick tissues were a challenge to image, due to pigmentation, autofluorescence and the density of tissue itself that would cause light scattering. And so, clearing techniques were raised to eliminate this problem and the first to be created were the solvent based clearing techniques that are based on an older technique of Spalteholz of delipidation and dehydration. But because the fluorescence

preservation was hard to achieve in solvent based techniques, aqueous-based clearing techniques were created as alternative methods.

IV.1.1. Tissue Clearing

For our work we tested several approaches in solvent-based and aqueous-based techniques to visualize organ vasculature in laser-scanning confocal and light-sheet microscopes. Testing these approaches, we concluded that delipidating approaches hardly give us good results for staining cell membranes, despite the compatibility that is described for each technique. This clearly demonstrates that each technique has to be individually optimized for the specific staining that is being used. Even though there are several membrane antibodies described in the PACT and iDISCO protocols that seemed to be compatible, our experiments and optimizations proved that immunostaining to ICAM2 is incompatible with these techniques, and an extremely sensitive epitope to work with. Aqueous-based techniques such as ClearT2 and CUBIC showed better compatibility. ClearT2 was selected as our control as it was the only technique in the first tests to show good staining results. Even though the first attempt to clear tissues with CUBIC showed us what we had already concluded, that delipidating reagents were damaging for membrane staining, after few modifications, the protocol turned out to be very efficient and compatible, showing very defined structures (with less noise and less dotty signal). ClearT2 is quite efficient when combined with perfusion of diluted Reagent 1, not just in terms of improving transparency, but it seems to also improve the signal/background ratio compared to the control (ClearT2). The background in the control technique might derive from lack of clearing achieved and possibly from the use of formamide itself that might damage the staining and/or increase background levels of autofluorescence. There are many techniques in the simple immersion approach that may enable a more efficient clearing than ClearT2 without damaging the staining (parallel experiments showed that formamide destroyed the staining of vessels with CD31/PECAM, another cytoplasmic membrane marker). Possible candidates could be FRUIT or TDE clearing techniques[41,50]. TDE clears tissue and the refractive index can be tuned by diluting it on water. FRUIT combines thioglycerol, fructose and urea for clearing (quite similar to Reagent 2); the FRUIT has improved tissue penetration and clearing derived from urea ability to hyperhydrate[38]. The clearing techniques in this category are weaker than hyperhydration or hydrogel embedding techniques, but acquiring thick tissue can be a combination of clearing and the type of microscopy applied.

IV.1.2. Microscopy

As shown in the previous experiments, confocal microscopy was able to acquire tissues with incomplete clearing, but the signal decays with depths and also there is the limitation in the working distance of the objectives we worked with that wouldn't allow us to scan for large 3D images. An

alternative to solve deep tissue light penetration is the two-photon microscopy. In this technique, fluorophores emitting in the visible range are excited by the absorption of two photons in the far-red region in minimal volume (>800nm). The greater advantage of this method is that far-red photons scatter far less than 400-700nm photons in biological tissue and thus have enhanced penetration. As for resolution, while the confocal microscopy obtains highly resolved images through the use of a pinhole that excludes the out-of-focus scattered light, two-photon microscopy uses the confinement of nonlinear excitation at the focus plane[51], because excitation outside the focal plane is less probable with two-photon absorption in the far-red wavelength[52]. This microscopy is effective when samples are not well cleared, however, the lateral resolution is worse and it requires higher light intensity that leads to phototoxicity. Light-sheet microscopy, on the other hand, combines optical sectioning with multiview imaging allowing illumination of fluorophores only in that volume. However, this microscopy requires well cleared samples in order for the plane of light to be captured by the detection objective. The most effective microscopy method for whole-organ visualisation is the two-photon lightsheet microscopy[53].

Different tissues have distinct clearing procedures and properties. Brain tissue is, perhaps, one of the easiest organ to clear and its vascular network is quite easy to acquire, especially using the lightsheet. Kidney and intestine were acquired only with confocal microscopy. The kidney has a very complex and dense structure to be visualized in the lightsheet. The major bottleneck in large 3D imaging is the size of the samples and penetration depth. Large samples are challenging to acquire as it generates a very large volume of data, putting a big pressure in terms of computing requirements for data handling and visualisation.

IV.2. Image analysis

After achieving successful staining of the golgi in well cleared organs, polarity analysis became possible in organs. In our initial experiments, the signal of golgi and nucleus becomes mixed up and the images can be very confusing in order to draw the polarity vectors, but nuclei and golgi distinction is possible due to their different shape. Nevertheless, the script used in MatLab to draw the vectors was designed for 2D images, as it occurs in retina vasculature that consists in simple layer of vessels that can be assumed as a 2D vessel network. After a flow simulation analysis, the information would be crossed with the polarity analysis information to correlate the polarity in EC with the direction of the flow, that was proved before to be opposite. The same principle would be applied to the organs vascular network to correlate flow with polarity and, additionally, to the VEGF levels in organs and to take conclusions as to what is the influence of VEGF in EC polarization against the flow, and whether does it contribute to the tissue-specific patterning. But in organs, the complexity of structure doesn't allow for polarity analysis to be so simple and in its current format

the flow simulation doesn't work for 3D reconstructions. The next step is to create a script that allows drawing vectors and flow simulation in a three dimensional space. Only then we will be able to make pattern analysis of polarity.

IV.3. Future Perspectives

An advance was made in terms of 3D organ tissue visualization for polarity analysis. After overcoming 3D flow simulations and polarity direction problems, deciphering connections between VEGF levels in tissues and their influence in patterning will become possible. This type of 3D experiment for polarity analysis in order to elucidate tissue-specific patterning can be performed in wild-type tissues or tissues lacking a specific protein that may be related to the remodelling event or directly linked to polarity establishment.

Regarding vascular patterning, it is important to know that 3D architecture varies dramatically between organs since it relates with tissue-specific function and the role of circulation for that function. Kidney illustrates well the function/architecture relationship since 25% of the cardiac input goes directly for kidneys when they only comprise 0.4-0.5% of body mass. It was shown that PDGFB signalling timing (that leads to Mural cells recruitment and vessel maturation) is very important for correct arterial arborization and early expression of the PDGFB receptor in VMC, which leads to early maturation, can dramatically alter the arborization and consequently impair kidney function[54]. Recalling what was said in the introduction, shear stress is the inducer of remodelling event, that instructs the patterning, and among the mechanosensors of the shear stress primary cilia are very important. Primary cilia have important signaling pathways that regulate migration, and planar cell polarity, such as PDGFRa, Wnt, hedgehog (Hg) and polycystins (PC)[55]. Take for instance PC-1 and PC-2 that are present in the primary cilia, disruption of any of these two proteins leads to a Autossomic Dominant Polycistic kidney disease (ADPKD), characterized by appearance of cysts derived from the nephronic epithelial. One of the symptoms, even though not frequent, is the appearance of aneurysms. Studies show that the cyst walls are highly vascularized, have high secretion of VEGF isoform 165 and expression of VEGFR2 and absence of VEGFR1, not to mention highly permeable vessels (that allow fluid secretion into the cyst)[56]. Studies in knockout mice embryos revealed that ablation of PCs led to aberrations of the lymphatic vessel sprouting and migration pattern[57]. Also, primary cilia modulate the expression of KLF2, which is a shear stress induced transcription factor that attenuates cell migration and establishes a quiescent phenotype[58] and has also been demonstrated to direct the formation of stress fibers that are align with the direction of the flow[25]. Taken these facts together it would be interesting to study the influence of primary cilia for patterning formation, especially because primary cilia are present mainly near the bifurcations where flow is perturbed[59]. Studying the effect of each of the primary cilia signalling

pathways in our methods for studying EC polarization in whole-organs could help elucidate important unanswered questions.

Another point to take up in terms of patterning could be the Notch and VEGF signaling. Notch influences artery/vein specification and tip and stalk phenotype. Mosaic vascular bed in zebrafish show that Notch deficient cells adopt tip cell phenotype while cells[60] with constitutive expression of Notch adopt stalk phenotype[61]. Multiple components of the VEGFR family are regulated by Notch. It is possible that determining the tip and stalk phenotype will somehow influence patterning. Also Notch, Wnt and ANG/TIE pathways crosstalk to orchestrate vessel pruning. Regarding the ANG/TIE signaling, Tie2 is the receptor of angiopoetin (Ang) 1 and 2 and is important for vessel maturation and remodeling. Tie1 regulates Tie2 expression and is usually absent in quiescent EC. Tie1 expression is stimulated by low shear stress and its expression regulates the expression of Tie2 and KLF2 and counters Tie2 membrane presentation. KLF2 induces expression of Tie2 and downregulation of Ang2 (an inducer of apoptosis and of vessel regression). Deletion of Tie1 shows increased vessel regression. The balance between the expression of the two receptors is important for correct regression, being important remodeling and, therefore, patterning.

Further experiments to help us elucidate the role of VEGF and shear-stress for polarity establishment and patterning would rely not only on large 3D vascular pattern analysis, but would also rely on a much smaller scale type of experiments, using microfluidics. Microfluidic devices are platforms for cell culture that allow manipulation of small amount of fluids on channels (10^{-9} to 10^{-18} liters)[62] and also manipulation of local microenvironment. The devices' small size allows the use of very small quantities of sample and reagents, which leads to highly sensitive and resolved detections, not to mention the easiness of transportation[63]. Resorting to these devices to study the molecular competition between VEGF and flow in several conditions can answer several questions. The use of patterning techniques such as lithographys extends the spectrum of devices that can be used for approaching several subjects regarding the study of angiogenesis. For instance, besides the study of flow and VEGF competition, we could reproduce the vasculogenesis and angiogenesis and behold the formation of patterns *in vitro*[64]. Using microfluidics devices we can study up close the signaling occurring at microvessel development stage, using cell-lines fluorescent for a certain protein that we wish to follow and study its interactions using high resolution microscopy. This sort of follow up cannot be achieved in *in vivo* organ level.

Overall, many pathways are involved in angiogenesis and can influence the tissue-specific patterns and these pathways are competitive with each other. The mechanism underlying tissue pattern formation is still unknown, especially how the outcome of two possible competitive signals is decided.

Chapter IV - Bibliography

1. Herbert, S. P. & Stainier, D. Y. R. Molecular control of endothelial cell behaviour during blood vessel morphogenesis. *Nat. Rev. Mol. Cell Biol.* **12,** 551–564 (2011).

2. Carmeliet, P. Angiogenesis in life, disease and medicine. *Nature* **438,** 932–6 (2005).

3. Bergers, G. & Song, S. The role of pericytes in blood-vessel formation and maintenance. *Neuro. Oncol.* **7,** 452–464 (2005).

4. Hoeben, A. *et al.* Vascular endothelial growth factor and angiogenesis. *Pharmacol. Rev.* **56,** 549–580 (2004).

5. Friedl, P. & Gilmour, D. Collective cell migration in morphogenesis, regeneration and cancer. *Nat. Rev. Mol. Cell Biol.* **10,** 445–457 (2009).

6. Ferrara, N. *et al.* Heterozygous embryonic lethality induced by targeted inactivation of the VEGF gene. *Nature* **380,** 439–442 (1996).

7. Bautch, V. L. VEGF-directed blood vessel patterning: From cells to organism. *Cold Spring Harb. Perspect. Med.* **2,** (2012).

8. Ruhrberg, C. *et al.* Spatially restricted patterning cues provided by heparin-binding VEGF-A control blood vessel branching morphogenesis. *Genes Dev.* **16,** 2684–2698 (2002).

9. Gerhardt, H. *et al.* VEGF guides angiogenic sprouting utilizing endothelial tip cell filopodia. *J. Cell Biol.* **161,** 1163–1177 (2003).

10. Zovein, A. C. *et al.* ??1 Integrin Establishes Endothelial Cell Polarity and Arteriolar Lumen Formation via a Par3-Dependent Mechanism. *Dev. Cell* **18,** 39–51 (2010).

11. De Bock, K., Georgiadou, M. & Carmeliet, P. Role of endothelial cell metabolism in vessel sprouting. *Cell Metab.* **18,** 634–647 (2013).

12. Jakobsson, L., Bentley, K. & Gerhardt, H. VEGFRs and Notch: a dynamic collaboration in vascular patterning. *Biochem. Soc. Trans.* **37,** 1233–1236 (2009).

13. Chappell, J. C., Taylor, S. M., Ferrara, N. & Bautch, V. L. Local Guidance of Emerging Vessel Sprouts Requires Soluble Flt-1. *Dev. Cell* **17,** 377–386 (2009).

14. Simons, M., Gordon, E. & Claesson-welsh, L. Mechanisms and regulation of endothelial VEGF receptor signalling. *Nat. Publ. Gr.* **17,** 611–625 (2016).

15. Lucitti, J. L. *et al.* Vascular remodeling of the mouse yolk sac requires hemodynamic force. **3326,** 3317–3326 (2007).

16. LAURENCE BECK, J. & D'AMORE', P. A. development : *FASEB J.* **11,** 365–373 (2016).

17. Dzau, V. J. & Gibbons, G. H. Introduction: Vascular Remodeling: Mechanisms and Implications. *J. Cardiovasc. Pharmacol.* **21,** (1993).

18. Forster, R. E. Systemic hypoxia changes the organ-specific distribution of vascular endothelial growth factor and its receptors. **95,** 15809–15814 (1998).

19. Djonov, V., Baum, O. & Burri, P. H. Vascular remodeling by intussusceptive angiogenesis. *Cell Tissue Res.* **314,** 107–117 (2003).

20. Culver, J. C. & Dickinson, M. E. The effects of hemodynamic force on embryonic development. *Microcirculation* **17,** 164–178 (2010).

21. Franco, C. a. *et al.* Dynamic Endothelial Cell Rearrangements Drive Developmental Vessel Regression. *PLOS Biol.* **13,** e1002125 (2015).

22. Korn, C. & Augustin, H. G. Mechanisms of Vessel Pruning and Regression. *Dev. Cell* **34,** 5–17 (2015).

23. Tzima, E. *et al.* A mechanosensory complex that mediates the endothelial cell response to fluid shear stress. *Nature* **437,** 426–431 (2005).

24. Hahn, C. & Schwartz, M. a. Mechanotransduction in vascular physiology and atherogenesis. *Nat. Rev. Mol. Cell Biol.* **10,** 53–62 (2009).

25. Boon, R. a *et al.* KLF2-induced actin shear fibers control both alignment to flow and JNK signaling in vascular endothelium. *Blood* **115,** 2533–42 (2010).

26. Li, J. *et al.* Piezo1 integration of vascular architecture with physiological force. *Nature* **515,** 279–282 (2014).

27. Satir, P., Pedersen, L. B. & Christensen, S. T. The primary cilium at a glance. *J. Cell Sci.* **123,** 499–503 (2010).

28. Suzuki, A. & Ohno, S. The PAR-aPKC system: lessons in polarity. *J. Cell Sci.* **119,** 979–987 (2006).

29. Drubin, D. *Cell Polarity*. (2000). doi:10.1007/978-3-319-14466-5

30. Zallen, J. a. Planar Polarity and Tissue Morphogenesis. *Cell* **129,** 1051–1063 (2007).

31. Nelson, W. J. Adaptation of core mechanisms to generate cell polarity. *Nature* **422,** 766–774 (2003).

32. Vorhagen, S. & Niessen, C. M. Mammalian aPKC/Par polarity complex mediated regulation of epithelial division orientation and cell fate. *Exp. Cell Res.* **328,** 296–302 (2014).

33. Goehring, N. W. PAR polarity: From complexity to design Principles. *Exp. Cell Res.* **8,** (2014).

34. Etienne-Manneville, S. Cdc42--the centre of polarity. *J. Cell Sci.* **117,** 1291–1300 (2004).

35. Iden, S. & Collard, J. G. Crosstalk between small GTPases and polarity proteins in cell polarization. *Nat. Rev. Mol. Cell Biol.* **9,** 846–859 (2008).

36. Wang, Y. & Nathans, J. Tissue/planar cell polarity in vertebrates: new insights and new questions. *Development* **134,** 647–58 (2007).

37. Schlessinger, K., McManus, E. J. & Hall, A. Cdc42 and noncanonical Wnt signal transduction pathways cooperate to promote cell polarity. *J. Cell Biol.* **178,** 355–361 (2007).

38. Richardson, D. S. & Lichtman, J. W. Clarifying Tissue Clearing. *Cell* **162,** 246–257 (2015).

39. Renier, N. *et al.* iDISCO: A Simple, Rapid Method to Immunolabel Large Tissue Samples for Volume Imaging - suppl original. *Cell* **159,** (2014).

40. Kuwajima, T. *et al.* ClearT: a detergent- and solvent-free clearing method for neuronal and non-neuronal tissue. *Development* **140,** 1364–8 (2013).

41. Hou, B. *et al.* Scalable and DiI-compatible optical clearance of the mammalian brain. *Front. Neuroanat.* **9,** 19 (2015).

42. Tainaka, K. *et al.* Whole-Body Imaging with Single-Cell Resolution by Tissue Decolorization. *Cell* **159,** 911–924 (2014).

43. Tomer, R., Ye, L., Hsueh, B. & Deisseroth, K. Advanced CLARITY for rapid and high-resolution imaging of intact tissues. *Nat. Protoc.* **9,** 1682–97 (2014).

44. Yang, B. *et al.* Single-Cell Phenotyping within Transparent Intact Tissue through Whole-Body Clearing. *Cell* 1–14 (2014). doi:10.1016/j.cell.2014.07.017

45. Renier, N. *et al.* Resource iDISCO : A Simple , Rapid Method to Immunolabel Large Tissue Samples for Volume Imaging. *Cell* **Im,** 1–15 (2014).

46. Susaki, E. A. *et al.* Advanced CUBIC protocols for whole-brain and whole-body clearing and imaging. *Nat. Protoc.* **10,** 1709–27 (2015).

47. Santi, P. A. Light Sheet Fluorescence Microscopy A Review. *J. Histochem. Cytochem.* **59,** 129–138 (2011).

48. Guan, Y. Q., Cai, Y. Y., Zhang, X., Lee, Y. T. & Opas, M. Adaptive correction technique for 3D reconstruction of fluorescence microscopy images. *Microsc. Res. Tech.* **71,** 146–157 (2008).

49. Schmitt, S., Evers, J. F., Duch, C., Scholz, M. & Obermayer, K. New methods for the computer-assisted 3-D reconstruction of neurons from confocal image stacks. **23,** 1283–1298 (2004).

50. Aoyagi, Y., Kawakami, R., Osanai, H., Hibi, T. & Nemoto, T. A Rapid Optical Clearing Protocol Using 2,2'-Thiodiethanol for Microscopic Observation of Fixed Mouse Brain. *PLoS One* **10,** e0116280 (2015).

51. Lee, J. H. *et al.* Comparison of confocal microscopy and two-photon microscopy in mouse cornea invivo. *Exp. Eye Res.* **132,** 101–108 (2015).

52. Kim, D. *et al.* Two-photon absorbing dyes with minimal autofluorescence in tissue imaging: Application to in vivo imaging of amyloid-?? plaques with a negligible background signal. *J. Am. Chem. Soc.* **137,** 6781–6789 (2015).

53. Mahou, P., Vermot, J., Beaurepaire, E. & Supatto, W. Multicolor two-photon light-sheet microscopy. *Nat. Methods* **11,** 600–601 (2014).

54. Hurtado, R. *et al.* Pbx1-dependent control of VMC differentiation kinetics underlies gross renal vascular patterning. *Development* **142,** 2653–2664 (2015).

55. Veland, I. R., Awan, A., Pedersen, L. B., Yoder, B. K. & Christensen, S. T. Primary Cilia and Signaling Pathways in Mammalian Development, Health and Disease. *Nephron Physiol.* **111,** p39–p53 (2009).

56. Bello-Reuss, E., Holubec, K. & Rajaraman, S. Angiogenesis in autosomal-dominant polycystic kidney disease. *Kidney Int.* **60,** 37–45 (2001).

57. Outeda, P. *et al.* Polycystin Signaling Is Required for Directed Endothelial Cell Migration and Lymphatic Development. *Cell Rep.* **7,** 634–644 (2014).

58. Dekker, R. J. *et al.* KLF2 provokes a gene expression pattern that establishes functional quiescent differentiation of the endothelium. *Blood* **107,** 4354–4363 (2006).

59. Egorova, a. D. *et al.* Lack of Primary Cilia Primes Shear-Induced Endothelial-to-Mesenchymal Transition. *Circ. Res.* **108,** 1093–1101 (2011).

60. Phng, L. *et al.* Dll4 signalling through Notch1 regulates formation of tip cells during angiogenesis. **445,** 2–6 (2007).

61. Siekmann, A. F. & Lawson, N. D. Notch signalling limits angiogenic cell behaviour in developing zebrafish arteries. **445,** 781–784 (2007).

62. Whitesides, G. M. The origins and the future of microfluidics. *Nature* **442,** 368–73 (2006).

63. Stone, H. A., Stroock, A. D. & Ajdari, A. ENGINEERING FLOWS IN SMALL DEVICESMicrofluidics Toward a Lab-on-a-Chip. *Annu. Rev. Fluid Mech.* **36,** 381–411 (2004).

64. Bichsel, C. a., Hall, S. R. R., Schmid, R. a., Guenat, O. T. & Geiser, T. Primary Human Lung Pericytes Support and Stabilize *In Vitro* Perfusable Microvessels. *Tissue Eng. Part A* **0,** 150529121444009 (2015).

65. Huisken, J. & Stainier, D. Y. R. Selective plane illumination microscopy techniques in developmental biology. *Development* **136,** 1963–1975 (2009).

66. Pries, A. R. & Secomb, T. W. Making Microvascular Networks Work : Angiogenesis , Remodeling , and Pruning Making Microvascular Networks Work : 446–455 (2016). doi:10.1152/physiol.00012.2014

Supplementary Information

Supplementary Table 1 - All clearing protocols tested

1st Tested protocols	Perfusion applied	Steps			
Solvent based Clearing					
iDISCO	Simple	Immunostaining	Dehydration	Delipidation	
Aqueous-Based clearing technique					
ClearT2	Simple	Immunostaining	Formamide / PEG		
PACT	Simple	Hybridization	SDS Clearing	Immunostaining	RIMS
CUBIC	CB-perfusion	Reagent 1	Immunostaining	Reagent 2	
Optimization					
8% SDS	Simple	8%SDS	Immunostaining	RIMS	
Immuno-SDS	Simple	Immunostaining	8%SDS	RIMS	
A4P0	Simple	Hybridization A4P0	immunostaining	Formamide/PEG	
Lectin Perfusion protocols					
Reagent 2	CB-perfusion	Pre-treat/Immunostaining	Reagent2	-	
Modified CUBIC	CB-perfusion	Post fixation	Reagent1	Pre-treat/Immunostaining	Reagent 2
Protocol 2	CB-perfusion	Post fixation	Pre-treat/Immunostaining	Reagent 1	Reagent 2
Other Protocols					
Modified CUBIC	CB-perfusion	Post fixation	Reagent 1	Pre-treat/Immunostaining	Reagent2
Protocol1	CB-perfusion	Post fixation	Pre-treat/Immunostaining	ClearT2	
Protocol2	CB-perfusion	Post fixation	Pre-treat/Immunostaining	Reagent1	Reagent2

All simple perfusions are followed by post-fixation 4°C overnight. All immunostainings after optimization tests have the pre-treatment (Pre-treat) step that was tested and revealed better staining results. CUBIC consists in a complex perfusion designated CB-perfusion followed by immediate immersion of organs in Reagent 1, followed by immunostaining and final clearing in Reagent 2; Modified CUBIC consists in adding a post fixation step after perfusion and only after PBS 1x washes immersion in Reagent 1; Protocol 2 is another modification of CUBIC in which immunostaining is performed first, fixed and only after the tissues are cleared; Reagent 2 was an experiment to test if clearing by Reagent 2 was sufficient in order not to clear with Reagent 1, the dilapidating reagent. Protocol 1 was a test to see if Clearing by ClearT2 could be improved by applying CB-perfusion.

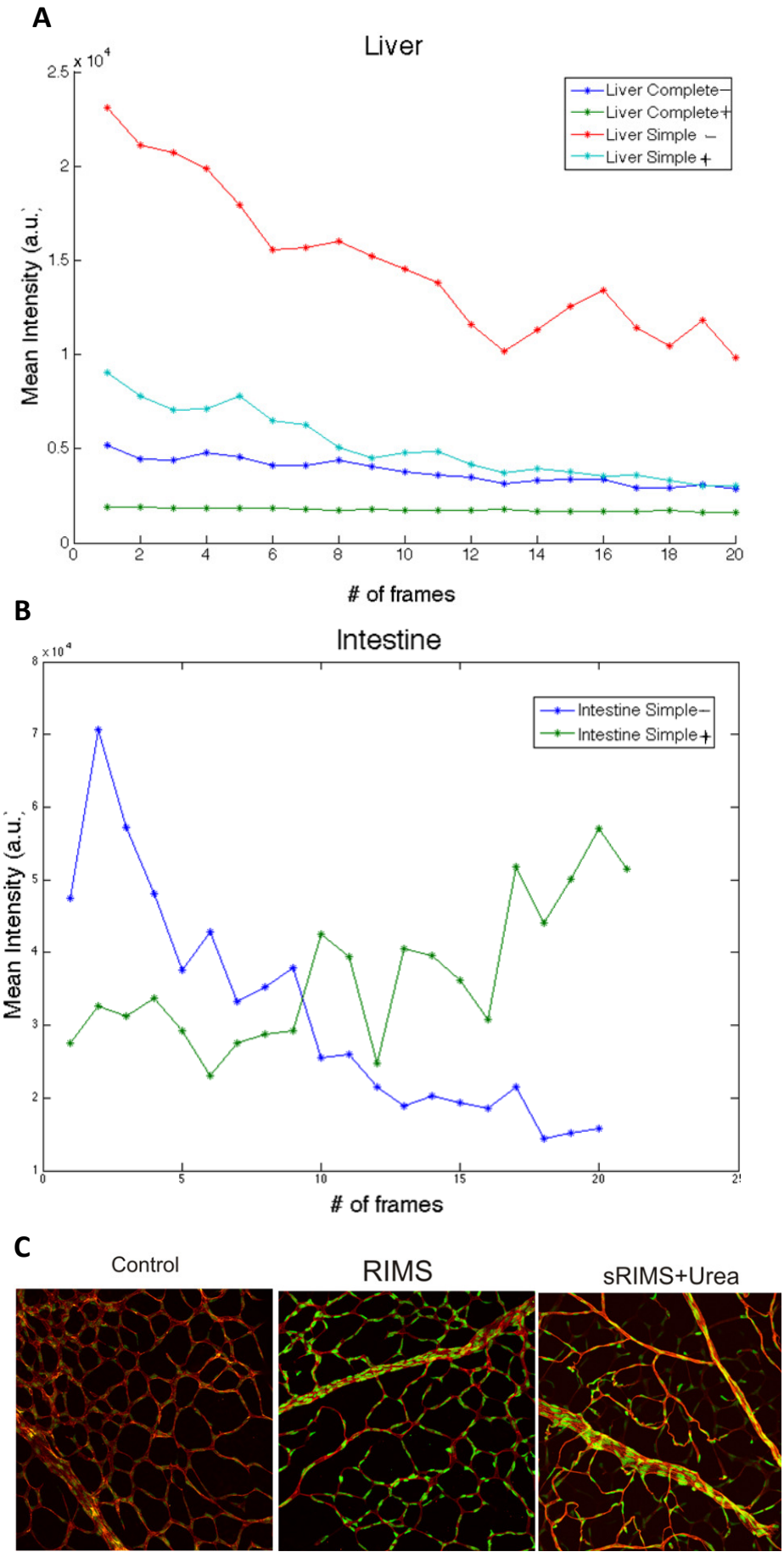

Supplementary Figure 1 - Urea test in Pre-treatment. A) and B) are graphs that represent the mean intensity of the ERG channel in liver and intestine tissue. To test if Urea could improve antibody penetration and improve the signal. In A) the red and green lines represent a liver that was cleared with CUBIC protocol (Complete) and had the pre-treatment in the presence of Urea or not (+ or -). The red and lighter blue lines represent the liver cleared with the normal ClearT2 protocol. In B) the signal intensity was only measured for intestine cleared by ClearT2. It is important to look at the decay of signal that can indicate the presence of signal. The decay can be due to lack of transparency that hampers signal penetration, but comparing the same protocols applied we can, perhaps, eliminate that variable. What we observe in the graphs is a higher decay of signal for tissues that went through pre-treatment without urea, while signal in tissues that were pre-treated in the presence of urea maintain a more or less constant signal. However in other tissues the intensity curves were highly variable and the conclusion as to the presence of urea being better remain inconclusive.

In C) we used retina, for their faster immunostaining protocols and natural transparency. Control retinas were observed in vectashield immersion medium. The other retinas were immersed in sRIMS and sRIMS containing urea in the same concentration as in the pre-treatment. The signal seems to be brighter in sRIMS+Urea, especially for ICAM signal. There were no direct evidences for improvement of antibody penetration due to the presence of urea, but because urea seems to give better signal quality we decided to maintain urea in the recipe.

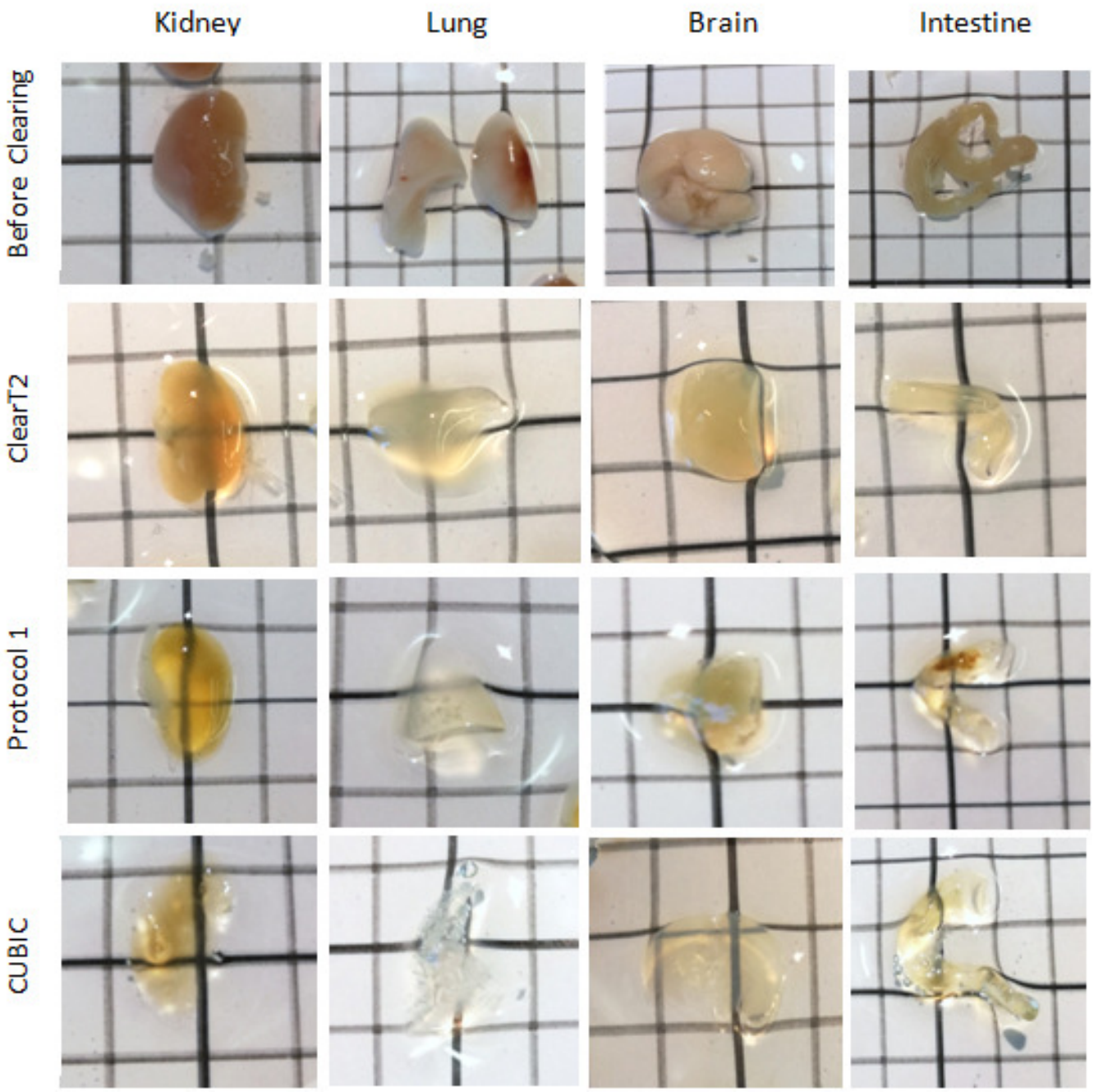

Supplementary Figure 2 - Cleared organs. ClearT2 is the control protocol. Protocol 1 is the combination of the CB-perfusion (from CUBIC protocol) and ClearT2. CUBIC is the clearing of the organs by Reagents 1 and 2. It is clear that an improved perfusion improves final clearing of the organs; Protocol 1 reveals better cleared organs than control. Nevertheless ClearT2 is a weak clearing protocol. CUBIC reveals better clearing efficiency. Because the samples were not completely immersed in the clearing media, there seems to be a "lens effect", seen as the distortion of the grid lines. Each square corresponds to 250mm^2.

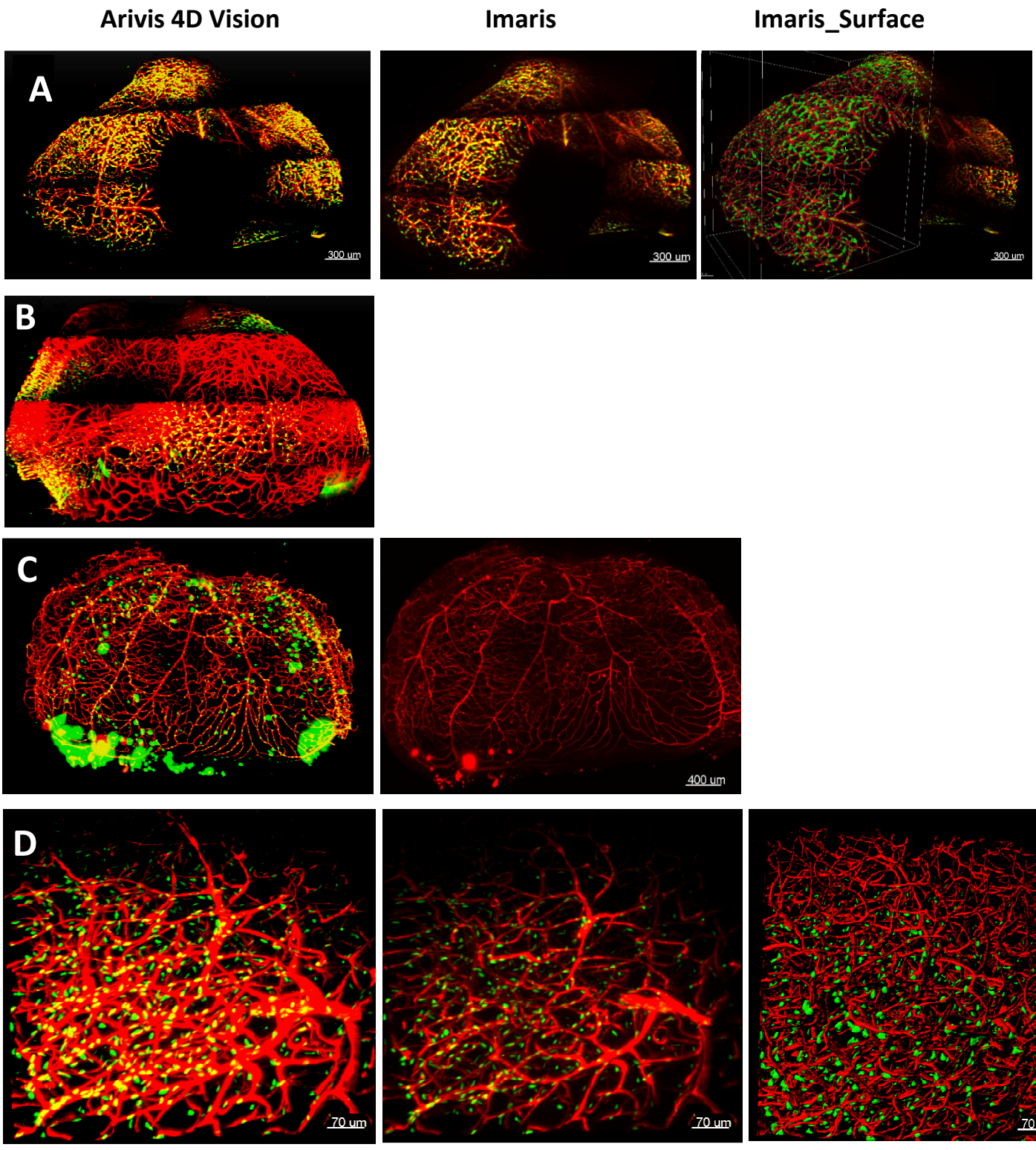

Supplementary Figure 3 - Testing the Lightsheet microscope. The column on the left are snapshots of the tissues in Arivis 4D Vision software. The middle column is the snapshot of tissues on Imaris and the right column are snapshots of the surfaces of vessels and nucleus created on Imaris. The tissues only were stained for ICAM2 and ERG. In A) is the first test of lightsheet acquisition with a retina, only a partial acquisition was made due to the size of data. B) The same retina was acquired fully, but processing became very difficult due to the size of data. C) Another retina acquired, but only half was acquired, using 40% overlapping tiles. D) The first test with organ tissue, brain, acquired without tile scan mode, only a simple Z-stack.

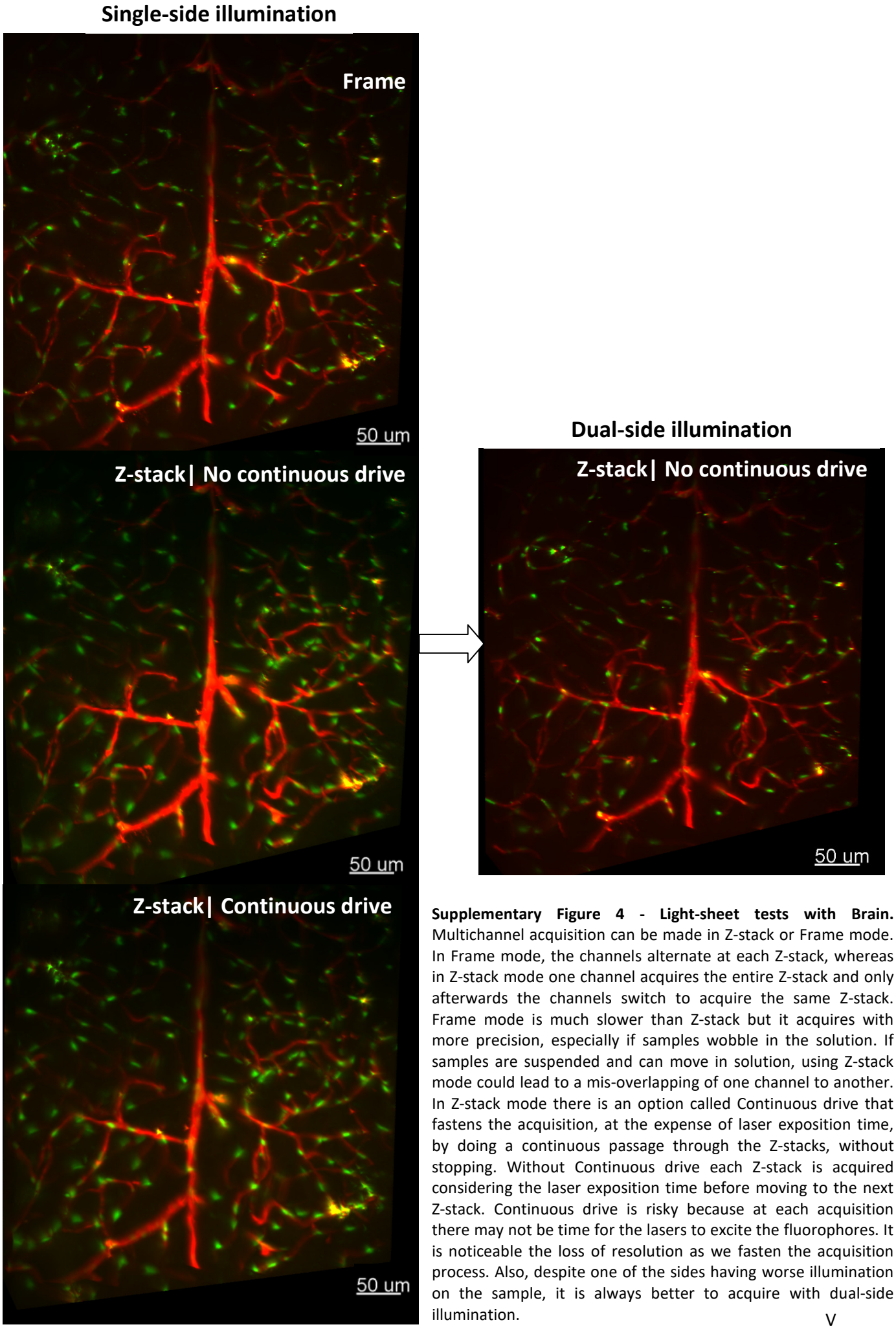

Supplementary Figure 4 - Light-sheet tests with Brain. Multichannel acquisition can be made in Z-stack or Frame mode. In Frame mode, the channels alternate at each Z-stack, whereas in Z-stack mode one channel acquires the entire Z-stack and only afterwards the channels switch to acquire the same Z-stack. Frame mode is much slower than Z-stack but it acquires with more precision, especially if samples wobble in the solution. If samples are suspended and can move in solution, using Z-stack mode could lead to a mis-overlapping of one channel to another. In Z-stack mode there is an option called Continuous drive that fastens the acquisition, at the expense of laser exposition time, by doing a continuous passage through the Z-stacks, without stopping. Without Continuous drive each Z-stack is acquired considering the laser exposition time before moving to the next Z-stack. Continuous drive is risky because at each acquisition there may not be time for the lasers to excite the fluorophores. It is noticeable the loss of resolution as we fasten the acquisition process. Also, despite one of the sides having worse illumination on the sample, it is always better to acquire with dual-side illumination.

Supplementary Table 2- Reagents Formulation.

Reagents	Components
PBS 10x (7.4)	8%(m/v) NaCl, 0,2%(m/v) KCl, 1,44%(m/v) Na_2HPO_4, 0,24%(m/v) KH_2PO_4
CBB	1%FBS, 3%BSA, 0,5% Triton-X-100, 0,01% Sodium Deoxycholate, 0,02% Sodium Azide in PBS1x (pH7.4)
Pre-treatment	1% Triton X-100, 0,5% Tween, 0,25% NP40, 0,25% Sodium Deoxycholate, 3% BSA and 1% Urea in PBS 1x (pH7.4)
Reagent 1	25 wt% urea, 25 wt% N,N,N',N'-tetra- kis(2-hydroxypropyl)ethylenediamine (Quadrol) and 15 wt% Triton X-100
Reagent 2	50wt% sucrose, 25 wt% urea, 10 wt% 2,20,20'-nitrilotriethanol (trietanolamine) and 0.1% (v/v) Triton X-100
RIMS	40g Histodenz in 30mL Phosphate buffer 0,02M, 0,1% Teen-20, 0,01% Sodium Azide
sRIMS	28g in 40mL Phosphate buffer 0,02M, 0,1% Teen-20, 0,01% Sodium Azide

Supplementary Table 3 - Z-step/Tissue Thickness (µm)

Figure 5	**iDISCO**	**ClearT2**	**PACT**	**CUBIC**	
Intestine	2/26	2/60	1.5/21	-	
Kidney	1.50/36	2/84	1.5/19.5	-	
Liver	-	-	-	3/57 and 6/66	
Figure 6	**Control**	**Pre-Treatment**	**SDS**	**Immune-SDS**	**A4P0**
Intestine	3.25/78.1	4.98/79,7	4.98/59.8	4.98/120	4.98/105
Kidney	4.11/98.6	4.98/64.7	1.93/19.5	-	4.98/64.7
Liver	2/56	-	-	2.25/54	-
Figure 7	**Control (ClearT2)**	**Protocol1**	**Protocol2**	**ModifiedCUBIC**	
Intestine	1.05/185	1.05/36.6	1.05/271	1.05/17.8	
Kidney	1.05/42.9	1.05/94.2	1.05/103	1.05/17.8	
Brain	1.05/67	1.05/85.8	1.05/162	1.05/38.7	
Figure 8	Brain	1.78/119	**Figure 12**	Kidney	0,672/13.4
	Kidney	1.49/7.44			

Supplementary Table 4 - System components.

Microscope	Magnification	Type	RI	Working distance (mm)
Confocal LSM 880	10x	Dry	1.0	5.2
	20x	Dry	1.0	0.55
Lightsheet	20x	Clear media	1.42 -1.48	5.6

Supplementary Table 5 - Refractive Indexes measured

Solution	Refractive Índex
Reagent1	1.4335
Reagent2	1.49
RIMS (1)	1.513
RIMS (2)	1.462
SRims	1.4432